Published in: Applied Geochemistry (2008), vol.23, iss.12, pp. 3819-3839
Status: Postprint (Author's version)

Long term mobilisation of chemical elements in tephra-rich peat (NE Iceland)

François De Vleeschouwer[a], Brigitte Van Vliët Lanoë[b,1] , Nathalie Fagel[a]

[a]*Unité de Recherche Argiles et Paléoclimats, Université de Liège, Allée du 6 Août, B18, Sart Tilman, B-4000 Liège, Belgium*
[b]*UMR 8110 CNRS Processus et Bilans des Domaines Sédimentaires, Université Sciences et des Technologies de Lille, SN5, B-59655 Villeneuve d'Ascq cédex, France*

Abstract

This paper presents geochemical profiles of a tephra-bearing minerotrophic peat column from NE-Iceland obtained using various elemental analyses of the solid phase and the pore water. The influence of tephra grain size, thickness and composition of each tephra on the peat geochemistry was investigated. Interpretations are supported by a statistical approach, in particular by autocorrelation, and by microscopy observations. Minerotrophic peat geochemistry may be strongly dependent upon post-depositional mobilization and possible leaching of elements as demonstrated by Fe and trace metal concentration profiles. Chemical elements, and more specifically potentially harmful metals, can be slowly leached out of volcanic falls during their weathering and re-accumulate downwards. It is emphasised that a tephra deposit can act as an active geochemical barrier, blocking downward elemental movements and leading to the formation of enriched layers. In this study, the formation of poorly amorphous Fe phases above the Hekla 3 tephra is shown. These poorly crystalline Fe phases scavenged Ni.

1. Introduction

Tephra is material ejected from a volcano to the atmosphere (Lowe and Hunt, 2001). Tephra can have a range of grain sizes, from plurimetric blocks to fine micrometric ash. The composition can vary between acidic ($[SiO_2] > 60\%$) and basic ($44\% < [SiO_2] < 52\%$). Basic tephras will be generally enriched in Fe and Mg. When dealing with aerial products resulting from magma projection in the atmosphere and rapid cooling, such as e.g. ignimbrites or ash falls, acidic tephras will generally be characterized by white and translucent glass shards (i.e. pumice), whereas basic ones will be darker (i.e. scoriae). Due to their grain size, the intensity of the volcanic explosion and the wind directions, tephra can be transported from very short to worldwide distances (Sparks et al., 1997). Volcanic deposits can strongly impact the surrounding environment (e.g. Holmes et al., 1999; Sadler and Grattan, 1999; Schmincke et al., 1999) in terms of immediate floral and faunal destruction (e.g. Hotes et al., 2004), and chemical changes (e.g. Haeckel et al., 2001; Flaathen and Gislason, 2007). Most of the studies dealing with the impact of volcanic falls have focused upon short time scales. For example, Flaathen and Gislason (2007) investigated the immediate impact of the 1991 and 2000 Mount Hekla eruptions in terms of major and selected trace element interaction between volcanic ash and surface waters. Few studies have dealt with the long-term impact of tephras, especially on plants and the organic environment. Research by Hotes et al. (2004) on mire vegetation in Hokkaido, Japan, showed that the principal factors affecting mire vegetation and chemistry were tephra thickness and grain size rather than tephra composition, pH or electrical conductivity. However, the mobilisation of metals from tephra layers deposited in peatlands has not been extensively studied, especially on millennial timescales, despite the fact that possible slow leaching of chemical elements may occur in acidic environments such as peatlands (Gislason and Oelkers, 2003; Pollard et al., 2003). In this study, by combining geochemical and micromorphological data on tephra of different composition, grain size and age, it is aimed to: (1) determine the principal factors affecting individual chemical behaviour, (2) identify possible post-depositional mobilization of chemical elements, (3) depict the possible particle-to-pore-water geochemical exchange, and mineral neo-formation, and (4) assess the influence of each tephra on the peat geochemistry over a millennial time scale. In order to achieve these objectives, results are presented from an Icelandic peat column containing several tephra deposits spanning a 4-ka period. The inorganic, major and trace element trends in the solid phase and extracted pore-waters were investigated. This geochemical study is combined with microscopy

[1] Present address: UMR 6538 Domaines Océaniques, Institut Universitaire Européen de la Mer, Place Nicolas Copernic, 29280 Plouzané, Bretagne, France.

analyses.

2. Site location and description

The Vesturárdalur valley is situated near Vopnafjördur, in NE Iceland. This region is mainly composed of peat- and grasslands lying on glacial deposits. The thickness of peat deposits in the Vesturárdalur valley is relatively shallow (max. 2 m). The position of Iceland on the Mid-Atlantic Ridge and above a volcanic hotspot leads to intense volcanic activity. Icelandic volcanic systems have emitted products from basic to acidic composition resulting from various magma processes. The principal tephras found in the Vopnafjördur area originated from the Hekla, Veidivötn and Oraefajökull volcanic systems (e.g. Thorarinsson, 1958, 1967; Larsen and Thorarinsson, 1977; Larsen et al., 1999, 2002; Eiríksson et al., 2004). Peat- and wetlands have also been continuously affected during their growth by aeolian particles coming from inland deserts.

As a great amount of material was needed for this study, and as numerous tephra layers could make any coring very difficult, it was decided to chose an outcrop and to take samples from it. The outcrop (ICE2) was selected on the basis of its maximum thickness (ca. 1.20 m). The present day peat vegetation is composed of mosses (*Aulacomnium palustre*), *Sphagnum* sp. (*Sphagnum teres*, *Sphagnum warnstorfii*), mostly *Cyperaceae* with some *Eriophorum angustifolium* and *E. scheuchzeri*, several *Carex* sp., *Juncaceae* (*Juncus alpinoarticulatus*, *Juncus filiformis*, *Juncus bufonius*), horsetail (*Hippuris vulgaris*) and few *Graminaceae* (http:// www.floraislands.is/engflora.htm). Given the vegetation dominance, the important continuous mineral input from volcanism (see below) and the pH, this peatland can be considered to be minerotrophic.

This region has a mean annual rainfall of ca. 800 mm/ a, with the lowest precipitation (30 mm/month) during April and May and the maximum (ca. 100 mm/month) between July and December. The mean annual temperature of the area is 4 ·C with maxima (ca. 10 °C) during June and August, and minima (ca. 0 °C) from December to April. Soil temperature is however higher than air temperature (ca. 5 °C in winter). The peatland is mostly rainwater fed. However, (sub-) surface runoff was observed within the top 10 cm of the outcrop. Sporadic pore-water samples collected at various depths in the profile and directly measured using pH paper revealed a pH of ca.5.5. Although the hydrological status of the present site was not investigated in detail, it can be compared to Sub-arctic peatlands, in the absence of permafrost. The combination of low water viscosity (due to low annual temperature and snow melt) with the presence of tephra in the outcrop ensures that little vertical movement occurs. Moreover, the parent material below the peat in the investigated area is a compact lodgement till (Fig. 1), which limits the vertical percolation loss and will therefore facilitate water saturation, as also stressed for most Arctic peats by Woo and Young (2006). The snow cover in Northern Iceland is specifically unstable in relation to brief warming periods related to cyclonic conditions and to wind remobilisation during cold events (catabatic winds from the South). On N-W facing slopes, this snow cover is around 1 m thick (A. Gudmundsson, pers. com.), mostly insulating the ground from frost penetration. During the melting season (March to late July), the lateral seepage of melt water from the overlying snow-patches buffers the temperature close to 0 °C in the peat superficial moss-root layer, except during occasional sunny days. As the ground below is warmer (ca. +5.5 °C MAGT), the spring inverted thermal gradient (inverted suction) together with the low water viscosity (i.e. 1.798 centipoise at 0 °C; 1.5188 centipoise at 5 °C and 1.3077 centipoise at 10 °C) limits the efficiency of possible downward water movement. Due to these conditions, feeding of the peat mass, even by lateral water movement is thus strongly limited. This was also supported by the limited water seepage from the deep horizons in the peat observed on the outcrop. Moreover the occurrence of a capillary barrier built by the contact between the H3 tephra and compacted peat (see Section 5.5) will promote slow lateral water migration. Although water flow rates were not measured, a maximum speed of lateral to slightly oblique drainage of 0.25-1 cm/s^{-1} can be estimated in superficial horizons from previous published studies in other sites (Blodeau and Moore, 2002; Daniels et al., 1977). However, the flow will be slower in deeper layers primarily because of peat humification and compaction, and to a lesser extent because of blocking of tephra pores by bacterial gels and mineral neosynthesis.

3. Sampling and preparation

3.1. Cutting and sub-sampling

As peat which outcrops may be affected by air conditions, a ca. 70 cm-deep trench was dug and cleaned, and a peat column was cut into the peat face which was not in direct contact with the air. The column was ca. 1.2 m in height and recorded five main tephra layers. Monoliths were cut using a stainless steel knife, wrapped in plastic film and PVC boxes (20 × 10 × 7 cm) and retrieved from the outcrop using a nylon cord. Two mm of external peat were removed from every monolith prior to sub-sampling to avoid any contamination. Ten-cm-long by 1-

cm-thick undisturbed slices were retrieved along the side of the box samples and were impregnated with resin for thin section preparation. The remaining box profiles were cut into 1 cm thick samples using plastic cutters and spatulas, which were cleaned using methanol and mQ water after each sample, to avoid cross-contamination. Except those designed for impregnation, all samples were processed in the same way: (1) pore-water extraction and analysis; (2) solid fraction analysis.

Fig. 1: *Above: map of Vopnafjördur area where ICE 2 was sampled. Below: detail of ICE 2 outcrop showing a grey gleyed ash (1), two white ashes (2 and white arrow), two oxidized black scoria layers (3 and 4). Five cryptotephras (C1-C5) were also detected on thin sections (De Vleeschouwer et al., 2008).*

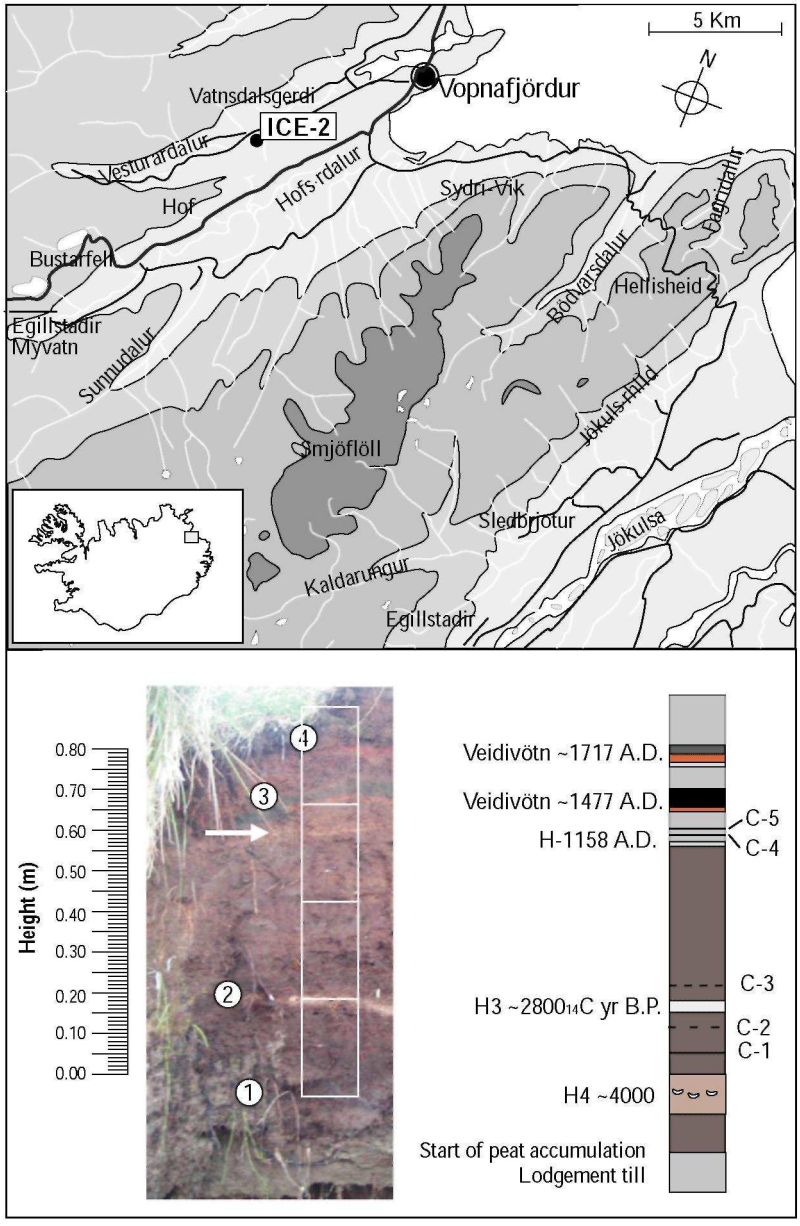

3.2. Pore-water extraction

Pore-water was collected from each sample (ca. 50cm^3) by refrigerated ultra-centrifugation (15,000 rpm, 10 °C) in PE tubes. Between each sample, tubes were cleaned using tap water followed by mQ water, and dried with lab clean paper. The extracted water was then directly transferred to 10 mL tubes and decanted. Two mL were sub-sampled for anion analysis. Then, 5 mL were finally sub-sampled and acidified using HNO_3 1 M for cation analyses. Water samples were analysed within a week to minimize possible chemical changes. This technique

offered the highest efficiency of pore-water extraction, and was the least time consuming when dealing with the large number of samples. However, ultra-centrifugation was critical for PO_4^{3-} and to a lesser extent for NO_3^- species as extraction was achieved in the open atmosphere (Shotyk, 1993; Steinmann and Shotyk, 1995). The extraction and cleaning processes were also critical for Zn contamination (J. Navez, pers. comm.). Values of PO_4^{3-} , NO_3^- and Zn are therefore at the very least semi-quantitative, but provided an effective guide for the relative fluctuation of these elements. It may also explain why pore-water Zn and PO_4^{3-} measurements are frequently inaccurate.

3.3. Solid phase preparation and treatment

After pore-water extraction, the dried samples were crushed manually using an agate mortar and then mechanically in an agatejar pulverisette (400 rpm, 1 h, mean grain size ~70 µm). About 1 g of each peat sample was dried (105 °C, 12 h) and burned (550 °C, 5 h) to estimate the loss on ignition (LOI).

In order to provide a continuous visual control of the sediment, undisturbed samples cut along the entire profile were impregnated in order to consolidate them prior to the preparation of thin sections. The method of impregnation is described in detail by Boës and Fagel (2005) and De Vleeschouwer et al. (2008). The basic steps are: (1) water removal (i.e. freeze-drying), (2) resin impregnation and (3) drying, sawing and thin-section preparation.

4. Analytical techniques

4.1. X-ray fluorescence of solid phase

For each sample, about 3.5 g of peat powder was pressed into pellets at 200 kN/cm^2. All the parts of the agate mortars were cleaned using tap water, methanol and mQ water, and dried using pressurized air between each sample. Pellets were analysed using a XRF spectrometer equipped with a Rh primary X-ray tube (ARL 9400 XP, URPGE, University of Liège) for the following elements: Si, Ti, AI, Fe, Mn, Mg, Ca, Na, K, Rb, Sr, Ni, Zn, Cu and Pb.

Two different calibrations were used for the major and the trace metals, respectively. For trace metals, several international reference samples with organic- and moderate silica-matrix were used to build up elemental calibration lines. These reference samples were coals (CLB-1, NIST 1632b), lichen (BCR-482), pond sediments (NIES-2), tea leaves (NIES-7), vehicle exhaust particulates (NIES-8) and marine sediments (JSD-2, JSD-3, SGR 44). All reference samples were first analysed to estimate the mean background on XRF analysis and to calculate the mean detection limit (DL) for each element. Sediment reference samples and vehicle exhaust particles were used to increase the range of values to high levels of elements possibly encountered in recent polluted peat layers. Statistics on reference samples are given in Appendix A.

For major elements, tests using the same international reference samples did not give accurate calibration lines. Two trend lines appeared for the organic and inorganic reference samples, respectively, reflecting matrix discrepancies between these two kinds of sediments. An alternative calibration line was thus built up for major elements using commercial low concentration Sphagnum peat spiked with ultrapure major elements. First, in order to quantify the major elemental content of the commercial peat, a peat internal standard (PIS) was prepared and repeatedly measured as follows: (1) a representative amount (~200 g) of the commercial low concentration Sphagnum peat was dried and homogenized; (2) five aliquots (~1 g) of this peat internal standard (PIS 1-5) were ashed, acid digested (HF + HNO_3) and analysed for major elements by ICP-AES (Iris Advantage, Thermo Jarrel Ash Co., MRAC Tervuren). Results are reported in Appendix B. Then, in order to reach maximum concentrations commonly encountered in peat in volcanic environments, a known amount of PIS was mixed with a known amount of the major elements, single oxides or carbonates (both ultrapure Merck quality). A part of this powder (PISAM 1, see Appendix B) was divided and diluted by ~1.5, 3, 6, 12 and 24 times (PISAM 1, 2, 3, 4 and 5, respectively). For each sample (PISAM 0-5), two pellets were prepared and one aliquot was ashed, acid digested and measured by ICP-AES. The SiO_2 content was estimated as: [% SiO_2] = 100 - ∑[% oxides] for both PIS and PISAM standards. Values of PISAM 0-5 were used as internal reference values to build major element calibration curves. Statistics on major elements are given in Appendix B.

4.2. Pore-water analysis

Cation concentrations in pore-water were measured using HR-ICP-MS (Finnigan Element 2, MRAC, Tervuren) for the following elements: Ti, AI, Fe, Mn, Mg, Ca, Na, P, Sr, Ni, Zn, Cu and Pb. Calibrations were made using

eight artificial solutions, three for major and five for trace elements. In addition, an international reference sample (SLRS 4, riverine water) was used to assess reproducibility and accuracy. Reproducibility values are between 93% and 97%. Accuracy values are below 10% for Na, Mg, AI, Ca, V, Cr and Fe, and between 10% and 20% for Cd, Pb, Mn, Co, Ni and Cu.

Anions were measured using ion chromatography (DIO-NEX DX100, DSTE-ULB) for Cl^-, NO_3^-, SO_4^{2-}, PO_4^{3-} simultaneously on 500 IL samples. The retention times of elution were $Cl^- < NO_3^- < PO_4^{3-} < SO_4^{2-}$. Calibration curves were built for each day of analysis using artificial solutions (Merck quality). Reproducibility values are above 98% for NO_3^-; PO_4^{3-} and SO_4^{2-}, and between 55% and 70% for Cl^-. Accuracy values are below 10% for NO_3^-, PO_4^{3-} and SO_4^{2-}, and above 10% for Cl^-.

4.3. Scanning electron microscope with energy dispersive system (SEM-EDS)

A few polished impregnated samples were C coated and analysed for major element content, without any re-sampling. The EDS used was a Quanta 200 ESEM (USTL, Lille) with a ROENTEC SDD xflash 3001 diode of 5 mm^2 and a working distance of 10 mm. Calibration was achieved using the ZAF protocol. Each elemental spectrum is compared with a spectrum obtained using an internal standard database (one spectrum per element). The precision varies with respect to atomic mass and applied voltage. Concentrations can be considered to be quantitative using point analysis, with an average error of 0.2%. EDS analyses were mainly performed on glass shards, scoria and alteration products. Results are reported in Table 1.

Table 1: *EDS analyses performed on shards from H3 (white ash, 17.5 cm height), V-1477 (black scoria, 68.5 cm height) and poorly crystalline Fe phases. REM stands for remarks (i.e. other particular elements detected). Concentrations in wt%.*

Section number	**Sample type**	**SiO_2**	**TiO_2**	**Al_2O_3**	**FeO_t**	**MgO**	**CaO**	**Na_2O**	**K_2O**	**REM**
ICE2 H3	Glass	70.58	0.34	15.95	5.47	0.37	2.79	2.39	2.11	-
	Altered glass	69.66	0.21	15.66	4.06	0.43	2.33	5.31	2.03	-
	Cracked glass	70.42	0.34	15.58	3.67	0.41	2.48	4.53	2.56	
	Cracked glass	74.02	0.27	15.03	2.51	0.28	1.67	3.82	2.40	-
ICE2 V-1477	Scoria	51.98	1.39	14.87	10.81	7.48	11.06	2.21	0.21	-
	Scoria	50.64	3.33	14.39	11.92	6.64	9.30	3.22	0.56	-
	Alterated scoria	51.95	1.13	4.64	9.18	16.33	15.91	0.71	0.15	-
Poorly crystalline Fe phases	High Fe	39.1	0.92	20.3	27.8	9.58	1.06	0.47	0.2	SO_3: 0.59
	Moderate Fe	44.6	7.26	32.9	12.1	0.75	1.78	0.59	-	-
	Low Fe	14.0	1.88	16.1	2.77	0.24	0.99	0.2	0.19	CO_2: 63.70

4.4. Autocorrelation

Autocorrelation is mainly used to discuss the influence of tephra falls on peat geochemistry. Numerous authors have used statistics in geochemistry. However, care should be taken when deducing interpretation from autocorrelation as the clear limit between simple visual relationship and real statistical correlation is rather vague in Earth Sciences. The interpretation of the correlation significance is variable from one author to another (e.g. Jin et al., 2006; Warren et al., 2006; Carboa et al., 2005; Price et al., 2005; Weiss et al., 2002) or even within a single article (e.g. Johnson et al., 2006; Todorova et al., 2005). "Strong" correlation is however generally accepted once *r* is lower than · 0.8 or higher than 0.8.

Attention is also drawn to the fact that it is not because the correlation coefficient *r* is elevated, that one parameter is responsible for the behaviour of another. Several parameters could also display the same behaviour, despite independent causes.

5. Results and discussion

The role of tephra on peat geochemistry will be discussed with regard to: (1) the ability of tephra to block and retain chemical elements and (2) possible tephra leaching. The tephra parameters which have the greatest influence on peat geochemistry will also be evaluated.

5.1. Tephrostratigraphy

The stratigraphy of tephras in ICE2 was established using previous tephrostratigraphical studies (e.g. Larsen and Thorarinsson, 1977; Boygle, 1999; Larsen et al., 1999, 2002; Lacasse, 2001; Wastegård, 2002; Eiríksson et al., 2004; De Vleeschouwer et al., 2008). The tephra deposits date back to 4 ka B.P. From the base to the top of the ICE2 outcrop, the first grey gleyified ash layer (Fig. 1) is Hekla H4 tephra (~4 ka B.P.), then in the middle part of the outcrop, the Hekla H3 white ash layer is recorded (~2.8 ka B.P.). Microscopy observation shows that this ash displays a particularly fine grain-size (5-20 µm) in the investigated outcrop. A second moderately fine grain-size (50-200 µm) white ash (H-1158, A.D. 1158; Fig. 1, arrowed) is also recorded in the ICE 2 outcrop, 10 cm below the lowest of two sub-centimetre black scoria layers (grain size: 50-200 µm), this latter being most likely the Veidivötn V-1477 A.D. tephra. This is confirmed by SEM analyses on single glass shards (Fig. 2). The discrepancies between the analyses and the Veidivötn field can be explained by the strong weathering of basic tephra which can make it difficult to achieve accurate analyses. The uppermost black scoria tephra (grain size: 50-100 µm) is the Veidivötn V-1717 A.D. This tephra is also commonly found in Icelandic lake and marine sediments. Five additional cryptotephras labelled C-1-C-5 (De Vleeschouwer et al., 2008) were identified by inspection of the thin sections.

Fig. 2: *Geochemical diagrams of Icelandic volcanic systems. Single grain analyses of 17.5 cm depth (H3) and 68.5 cm depth (Veidivötn 1477 A.D.) samples. H3 is represented in grey field, other tephra composition data are reported in white fields with corresponding names.*

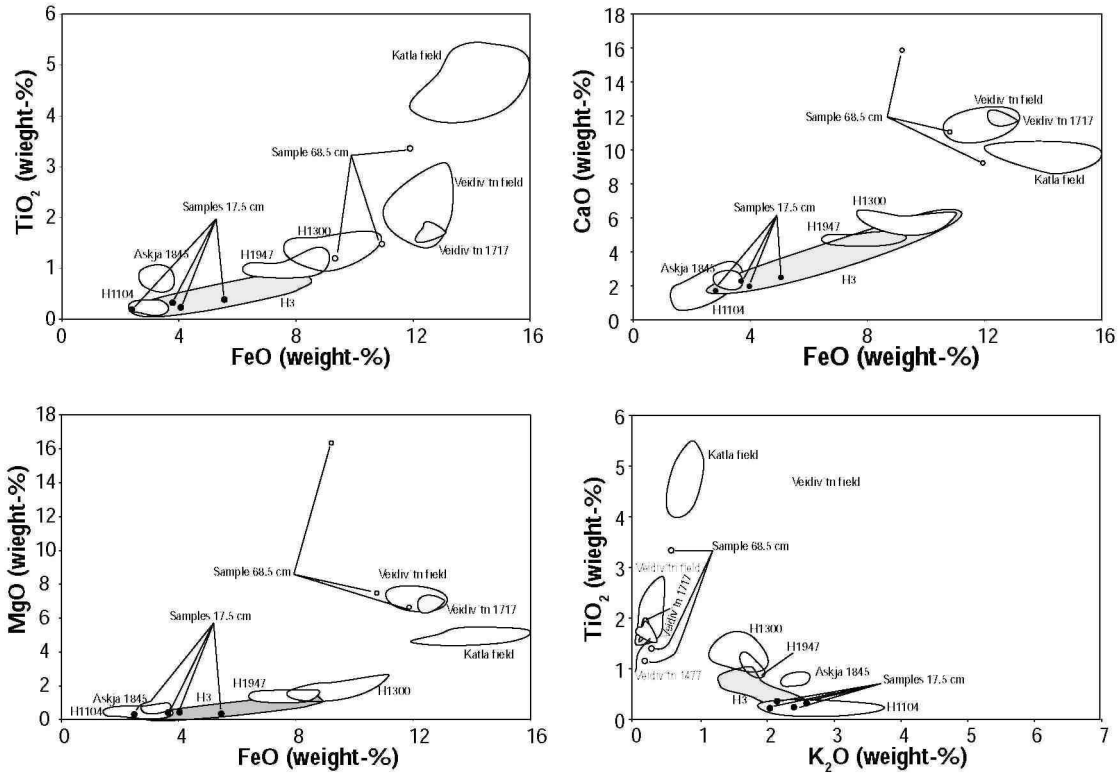

5.2. Peat geochemistry

Solid phase samples (Table 2) display rather high values of Al (median 3.4%), Ca (median 1.1%), Fe (median 2.0%) and Si (median 7.5%). These trends reflect the minerogenic characteristics of the peat, which receives continuous inputs of volcanic dust.

Compositional variations occur between the tephra deposits. For example, in H3, there are enrichments of Si and Al and depletion of Ca and Fe. Potassium displays low concentrations (<0.1%) except in and around the H3 ash, where concentrations are significantly higher, reaching 0.4% (Fig. 3). Magnesium concentrations are stable

around 0.4%, except in the two V-1477 and V-1717 scoriae layers, where this element is slightly enriched. Manganese and Na are below the detection limit (respectively, 0.04% and 0.4%). Trace metals have moderately high concentrations (median Cu = 4.7mg/kg, median Ni = 33.5 mg/kg, median Zn = 51.8 mg/kg), except Pb, which is always below the detection limit (i.e. <7.2 mg/kg). Rubidium and Sr show a strong increase in the H3 tephra compared to the peat layersjust below and above it. Nickel and Zn also show an increase in concentration above the H3 tephra deposit. Aluminium and Fe in pore-water display low concentrations, with respective median values of 97 and 147 µg/kg, although roughly peaking around the V-1477 and V-1717 scoria layer (Table 3). Calcium, Na and Mg concentrations in pore-water are much higher with median values of 17.7, 14.2, and 9.2 mg/kg, respectively. $Titanium_{pw}$ and Cu_{pw} roughly follow their respective solid phase profile, but peakjust under the V-1477 scoria. $Copper_{pw}$ also peaks under the V-1717 tephra. $Strontium_{pw}$ displays a flat profile, except in the uppermost parts where peaks occur just under the V-1477 and V-1717 tephra deposits.

5.3. Tephra leaching and metal release - a slow reaction

Observation of thin sections revealed alteration films around glass shards (see also De Vleeschouwer et al., 2008). However, no significant elemental leaching was found below the tephra layers, except slight leaching above V1477 and V1717 (Fig. 3). The mechanisms responsible for tephra leaching in waterlogged sediments have been abundantly studied (e.g. Wolff-Boenisch et al., 2004a,b; Pollard et al., 2003; Techer et al., 2001; Oelkers, 2001; Thorseth et al., 1995; Hodder et al., 1991). Glass shard dissolution depends first upon the glass composition. Silica structures in basaltic glass are less organized than in rhyolitic glass, leading to various dissolution rates. Wolff-Boenisch et al. (2004a,b) deduced the relationship between the lifetime of an idealized 1-mm-thick layer composed of 1-mm radius natural glass spheres and their silica content at far from equilibrium conditions. Such small tephras may take up to 4 ka to fully dissolve. Other parameters such as Eh-pH conditions, formation of alteration films at the surface of the glass shards (which prevent dissolution), and bacterial activities can also play a role. Among those, alteration films around grains play an important role in the blocking of elemental diffusion from the glass shard to the sediment (Techer et al., 2001).

A rough calculation of the quantity of chemical species a tephra will release can be performed, by estimating the difference between the metal concentration in fresh glass shards (from the literature) and the actual metal concentration in the tephra contained in the peat column normalized to the age of the tephra (see Table 4A). However, some elements such as Na have been leached out to below the detection limit, and leaching rates can thus not be calculated. The calculated release rate of Fe is the second most important (ca. 9 mg kg^{-1} a^{-1}) after Si (ca. 47 mg kg^{-1} a^{-1}). The following elements leached out are cations such as Ca (ca. 5 mg kg^{-1} a^{-1}), K (ca. 1 mg kg^{-1} a^{-1}) and Mg (ca. 0.6 mg kg^{-1} a^{-1}). These values are much higher than the values found by Wolff-Boenisch et al. (2004a) who found respective release rates of ca. 0.041 mg k^{-1} a^{-1}, 0.024 mg kg^{-1} a^{-1}, 0.019 mg kg^{-1} a^{-1} and 0.003 mg kg^{-1} a^{-1} for Fe, Ca, K and Mg, respectively (re-calculated from Fig. 7 of Wolff-Boenisch et al., 2004a, using a glass density of 2.42 g cm^{-3} and a SiO_2 content of 66% found in the outcrop at 16.5 cm height). These discrepancies are due to the fact that: (1) tephra deposits were sampled together with the peat and (2) the bacterial effect and protective films around the glass shards (which are expected to decrease the dissolution rates) were not taken into account.

Table 2: *Concentrations in peat solid phase samples of ICE 2 peat outcrop measured by XRF (URPGE, ULg). DL: under the detection limit.*

Height (cm)	Al (%)	Ca (%)	Fe (%)	K (%)	Mg (%)	Si (%)	Ti (%)	Cu (mg/kg)	Rb (mg/kg)	Sr (mg/kg)	Ni (mg/kg)	Zn (mg/kg)
0.5	2.41	1.13	1.16	DL	0.27	4.84	0.26	1.52	4.67	60.34	24.66	17.61
1.5	2.12	1.09	1.15	DL	0.27	4.68	0.24	1.18	4.87	61.07	20.55	12.65
2.5	1.99	1.07	0.99	DL	0.26	4.50	0.24	DL	5.03	58.88	21.09	10.32
3.5	2.01	1.12	1.21	DL	0.27	4.88	0.24	1.09	4.46	56.97	21.35	11.53
4.5	1.91	1.11	1.37	DL	0.27	5.04	0.24	DL	4.77	52.97	21.28	10.49
5.5	1.89	1.04	1.37	DL	0.25	4.80	DL	DL	4.45	48.14	22.97	11.51
6.5	2.03	1.02	1.51	DL	0.25	5.06	DL	DL	4.29	45.18	23.58	11.76
7.5	2.21	0.96	1.81	DL	0.23	5.26	DL	DL	4.46	46.85	25.44	15.32
8.5	2.18	0.95	2.15	DL	0.23	4.88	DL	1.09	4.63	44.03	27.25	22.34
9.5	2.31	0.97	2.22	DL	0.24	4.97	DL	1.12	3.81	43.77	25.81	25.53
10.5	2.13	0.97	2.39	DL	0.24	4.64	DL	1.62	5.82	47.39	28.16	32.80
11.5	2.20	1.00	2.43	DL	0.25	4.69	DL	1.77	5.58	50.25	29.83	30.82
12.5	2.09	1.00	2.26	DL	0.25	4.48	DL	1.59	5.51	50.65	32.88	31.06

13.5	2.24	0.93	1.89	0.09	0.22	5.55	DL	1.39	6.90	48.89	32.94	27.87
14.5	3.24	0.70	1.40	0.28	0.17	9.71	DL	DL	17.37	84.73	28.68	37.98
15.5	3.44	0.64	1.22	0.33	0.15	10.70	DL	DL	20.37	92.82	25.53	38.46
16.5	3.85	0.57	1.22	0.39	0.13	12.13	DL	DL	25.83	110.37	25.88	44.34
17.5	4.04	0.56	1.30	0.41	0.13	12.51	DL	DL	27.76	119.83	25.28	51.45
18.5	3.79	0.58	1.41	0.36	0.14	11.21	DL	DL	24.22	104.15	31.72	51.63
19.5	4.01	0.59	1.49	0.37	0.15	11.80	DL	DL	25.38	111.23	30.40	58.95
20.5	3.44	0.73	1.81	0.25	0.20	8.95	DL	1.35	16.67	84.08	46.85	67.45
21.5	3.11	0.90	2.17	0.15	0.24	7.38	DL	2.54	10.21	68.78	55.23	63.96
22.5	2.77	0.90	2.27	0.08	0.24	6.19	DL	3.29	7.22	57.51	64.23	64.30
23.5	2.51	1.00	2.36	0.04	0.25	5.07	DL	3.36	5.68	51.26	73.26	52.42
24.5	2.71	1.02	2.67	DL	0.27	5.18	0.30	4.23	6.41	64.34	78.75	65.34
25.5	2.17	1.05	2.69	DL	0.24	3.43	0.27	4.31	4.85	47.84	64.71	42.13
26.5	2.33	0.96	2.89	DL	0.24	4.06	0.26	5.23	5.27	42.66	68.16	47.77
27.5	2.61	0.95	2.82	DL	0.26	4.69	0.26	5.44	5.49	47.82	65.36	53.37
28.5	3.32	0.98	2.07	DL	0.29	5.68	0.28	5.26	5.65	62.22	44.33	43.83
29.5	3.36	0.98	2.00	DL	0.29	5.51	0.31	5.44	5.85	61.68	40.99	39.84
32.5	4.04	1.00	1.51	0.04	0.30	5.91	0.49	4.63	6.05	81.22	39.49	45.54
33.5	4.17	1.07	1.43	0.04	0.34	6.22	0.47	4.67	6.51	82.82	38.20	40.29
34.5	4.20	1.10	1.37	0.04	0.36	6.28	0.42	4.69	5.75	80.90	34.85	39.43
35.5	3.94	1.09	1.27	0.05	0.35	6.42	0.38	4.21	6.98	80.65	35.79	41.64
36.5	4.23	1.14	1.36	0.05	0.34	7.00	0.42	4.50	6.59	77.34	32.33	42.61
37.5	4.23	1.18	1.40	0.05	0.37	7.08	0.40	4.31	6.69	77.44	34.90	47.09
39.0	3.95	1.18	1.44	0.05	0.37	6.96	0.37	4.29	6.59	74.21	32.07	47.98
40.5	3.13	1.13	1.56	0.05	0.31	6.18	0.29	3.13	6.47	70.64	27.29	50.73
41.5	3.13	1.03	1.52	0.05	0.31	5.66	0.28	3.80	7.38	85.34	31.01	58.58
42.5	3.94	1.25	1.85	0.05	0.39	6.99	0.31	4.62	7.35	96.52	34.39	62.87
43.5	3.75	1.21	1.90	0.04	0.39	7.55	0.29	4.90	6.80	86.10	33.58	60.95
44.5	3.35	1.10	1.88	DL	0.32	8.08	0.25	4.94	7.10	78.46	32.60	56.16
45.5	3.21	1.10	1.98	0.04	0.34	9.48	0.25	4.83	6.63	79.09	32.09	49.39
46.5	3.16	1.09	2.32	0.04	0.35	9.47	0.25	4.46	8.22	83.36	34.89	53.29
47.5	3.14	1.00	2.29	DL	0.28	9.30	0.27	4.50	7.18	80.55	33.38	54.60
48.5	3.45	1.10	2.12	0.04	0.34	8.78	0.30	4.65	8.24	98.76	35.80	58.21
49.5	3.71	1.25	1.73	0.05	0.43	8.27	0.34	4.68	8.14	113.00	38.79	62.06
50.5	3.66	1.26	1.58	0.05	0.41	8.38	0.31	5.00	8.51	104.98	39.55	58.25
51.5	3.86	1.23	1.45	0.05	0.40	8.15	0.34	5.96	7.88	103.42	41.63	56.47
52.5	4.29	1.24	1.54	0.06	0.41	8.42	0.45	5.45	8.28	124.47	43.13	70.44
53.5	4.49	1.22	1.55	0.07	0.41	8.19	0.52	5.09	8.78	139.70	39.68	79.28
54.5	4.85	1.18	1.59	0.06	0.39	8.24	0.54	5.24	9.31	137.21	35.26	81.48
55.5	4.28	1.08	1.99	0.05	0.35	8.71	0.38	5.82	8.47	93.21	32.68	51.96
56.5	4.19	0.97	2.62	0.04	0.38	11.21	0.34	5.74	6.90	75.37	27.41	50.07
57.5	4.07	0.72	2.86	DL	0.30	12.17	0.33	4.00	7.50	64.70	21.87	50.33
58.5	3.66	0.72	2.59	0.04	0.27	12.04	0.28	DL	DL	DL	DL	DL
59.5	4.08	1.11	2.56	0.08	0.37	11.07	0.29	DL	DL	DL	DL	DL
60.5	3.48	0.98	2.30	0.09	0.32	9.79	0.29	4.45	10.70	105.06	29.54	53.77
61.5	3.65	0.90	2.60	0.06	0.28	9.12	0.32	4.77	9.01	87.87	27.98	67.48
62.5	4.26	0.97	1.90	0.07	0.32	9.27	0.36	4.68	10.27	106.91	31.32	81.81
63.5	4.32	1.04	1.79	0.08	0.35	9.25	0.37	4.73	10.25	113.67	31.88	82.23
64.5	3.68	0.97	2.83	0.08	0.31	8.03	0.31	6.37	10.62	93.79	32.76	80.36
65.5	2.63	1.02	4.20	0.06	0.28	7.53	0.25	5.54	10.93	97.92	38.56	63.64
66.5	3.08	1.32	2.65	0.06	0.49	8.56	0.24	6.30	10.16	114.13	37.27	57.90
69.5	3.97	1.58	2.05	0.07	0.69	8.99	0.26	6.87	10.94	139.55	43.69	62.14
70.5	3.24	1.32	2.17	0.06	0.42	6.95	0.26	5.97	9.85	120.92	35.40	53.10
71.5	3.53	1.31	2.09	0.07	0.46	7.83	0.29	4.87	9.72	121.52	36.74	57.40
72.5	3.45	1.37	2.24	0.07	0.46	7.65	0.29	4.81	9.81	123.75	35.67	56.48
73.5	3.02	1.24	2.56	0.07	0.41	7.75	0.25	4.18	9.64	111.92	33.50	52.53
74.5	2.91	1.25	2.48	0.06	0.38	7.43	0.26	4.04	9.29	108.92	34.14	46.94
75.5	2.94	1.28	2.44	0.06	0.40	6.72	0.25	4.38	9.26	109.20	34.68	47.37
76.5	3.27	1.36	2.35	0.07	0.46	7.29	0.27	4.65	9.29	120.58	36.20	52.99
77.5	3.86	1.34	2.59	0.07	0.51	8.27	0.27	10.13	9.75	103.15	37.71	69.59

79.0	3.47	1.04	3.25	0.08	0.34	7.57	0.29	7.43	10.49	89.77	35.24	75.52

5.4. Tephra leaching or simple mix - the case of H1158 and Veidivötn tephras

Below H1158, Ca, Sr, Ni and K are correlated (Appendix E). Nickel is also positively correlated with Zn. Copper is positively correlated with Rb, Ni and, to a lesser extent, with Sr. A careful inspection of thin sections showed that the only feature causing this correlation is a transition from a peat with its own chemical composition to H1158. The progressive mix of particles from the peat (enriched in Ti, Ca, Al, Sr and Zn) to H1158 (depleted in Ti, Ca, Al, Sr and Zn relative to the peat) provokes simultaneous changes in the chemical profiles. In comparison, Fe and Si concentrations increase below the tephra and are strongly negatively correlated with the other elements, as these two elements are enriched in mineral phases from the tephra. Moreover, the maximum Ti concentration is in the peat below H1158. Titanium is generally considered immobile in soil profiles, which would suggest that the peak in concentrations (i.e. Ti, Ca, Al, Sr, Zn) is not the result of the leaching of elements from H1158. In pore-waters, two groups of elements are apparent. On one hand, Al_{pw}, Fe_{pw}, Ti_{pw} and to a lesser extent Cu_{pw} are correlated positively. These are enriched within H1158, suggesting partial cation leaching within the tephra. However, no post-depositional mobilisation can be found. This phenomenon is also found in Veidivötn A.D. 1477. Elemental mapping of V1477 also shows leaching of tephra and the formation of amorphous particles enriched in Fe and AI, compared to Si (Fig. 4).

5.5. Tephra as an active barrier - the case of H3 tephra

The study site is a stratified peat deposit formed on a gentle slope and the water flow is expected to be oblique. Nevertheless, the presence of tephra layers will promote the specific surface of their vacuoles to behave as a capillary barrier, impeding downward transmission of water, mostly by single capillary forces, and promoting water flow at its upper contact with the peat. Open vacuoles in the tephra also play a role as a specific microbial biotope with very slow water exchange, facilitating the weathering of basaltic grains. As no real true flow exists in a tephra layer, this pathway is slowly blocked by bacterial production, increasing the mechanical role of the capillary barrier. For this reason the development of bacterial gels with high exchange surface on the tephra favours the adsorption of metallic cations. Under these conditions, weathering of volcanic dust in the upper peat and on the surface slope due to the production of humic acids and bacterial production will lead to the release of cations, especially Fe from basaltic glasses.

In the peat column shown here, Fe is often enriched above and below tephra layers (Fig. 3). This is particularly the case above H3 (between 24.5 and 27.5 cm height), despite Hekla H-3 being a low to moderate Fe tephra compared to basic tephra like Veidivötn. The increase in metal content can be estimated by comparing the metal content in the peak (between 24.5 and 27.5 cm height) and its counterpart in the low concentration peat, which is assumed to represent the sediment which is less influenced by metal accumulation. Such layers are found between 32.5 and 40.5 cm height, where most of the chemical species analyzed display low values or flat profiles. Calculations show that the Fe content is enriched by 100%just above H3 (Table 4B), while other elements are depleted (enrichment factor <0%) or display no significant enrichment. Based on microscopic observation, the primary features found in thin section at around 25 cm height are oxyhydroxide patches (Fig. 5). Iron oxyhydroxides are highly mobile and common features in organic sediments under slightly acidic (pH 5-6) conditions (Cornell et al., 1989), which are the typical minerotrophic peat water conditions. These oxyhydroxides are commonly goethite in soils that have restricted drainage and form orange to light brown patches. Flaathen and Gislason (2007) also identified rapid amorphous FeOOH saturation in surface waters polluted by ash falls in Iceland. In addition a strong link between Fe and LOI implies that the poorly crystalline phase containing Fe could be partly organic. Iron hydroxides form by Eh modification due to the consumption of Fe(II) chelates by bacteria and local pH increases due to the weathering of basaltic glass. Moreover, because of the behaviour of the capillary barrier, the lowermost interface is aerated/oxidized. For this reason, the solubility of Fe decreases in favour of more oxidized forms. Another explanation could be that organic matter (i.e. mucus on cyanobacteria filaments) is adsorbing superficial Fe oxyhydroxide as observed by Soulier (1995). This adsorption of poorly crystalline Fe phases was also identified by Glasauer et al. (2002).

Nickel is also strongly enriched (91%), similar to Zn (ca. 15%) and Cu (ca. 8%) to a lesser extent (Table 4B). In pore-water, the same enrichments in Fe and Ni are observed. Correlation performed on 14 samples above Hekla H3 reveals a strong link between Fe, Ni and loss on ignition (LOI) with r ranging from 0.85 between LOI and Ni to 0.95 between Fe and Ni (Fig. 6, Table 1). In addition, a second cluster of elements (Al, Mg, Si, Ti, K, Mg and Sr) is recorded (see example of Si and Al in Fig. 6). These two groups of elements are clearly dependent on sediment mineralogy. On the one hand, the siliceous phase of the sediment is dominated by minerals and glass

shards found in siliceous tephras, while on the other hand, the clustering of Fe, Ni and LOI implies the occurrence of a non-siliceous phase containing Fe and Ni, which has a link with organic matter. The high correlation coefficient (r = 0.95) between Fe and Ni is in good agreement with the dissolved Fe migration from the upper layers to above H3 (20-25 cm) where it is blocked and precipitates. Indeed, H3 is a very compacted and very fine grained sized ash (5-20 µm, see Section 5.1), and could possibly be a physical barrier to dissolved species migrating downwards through the water column. The high correlation coefficients found between Fe_{pw}, Ca_{pw}, Mg_{pw}, Mn_{pw}, Ti_{pw}, and Ni_{pw}, above H3 support the hypothesis of a tephra barrier. Therefore H3 not only stops water percolation, but concentrates dissolved elements (Ca_{pw}, Fe_{pw}, Mg_{pw}, Mn_{pw}, Ti_{pw}, and to a lesser extent Al_{pw}) above the tephra. More specifically, Fe is blocked until its saturation, causing its precipitation and the subsequent adsorption of Ni onto freshly formed Fe, poorly crystalline particles.

Fig. 3: *Elemental profiles from ICE2. Concentrations are in mg/kg for the solid phase and for anions in pore-water, while in Ig/kg for cations in pore-water. Black circles are peat samples while open triangles are pore water samples.*

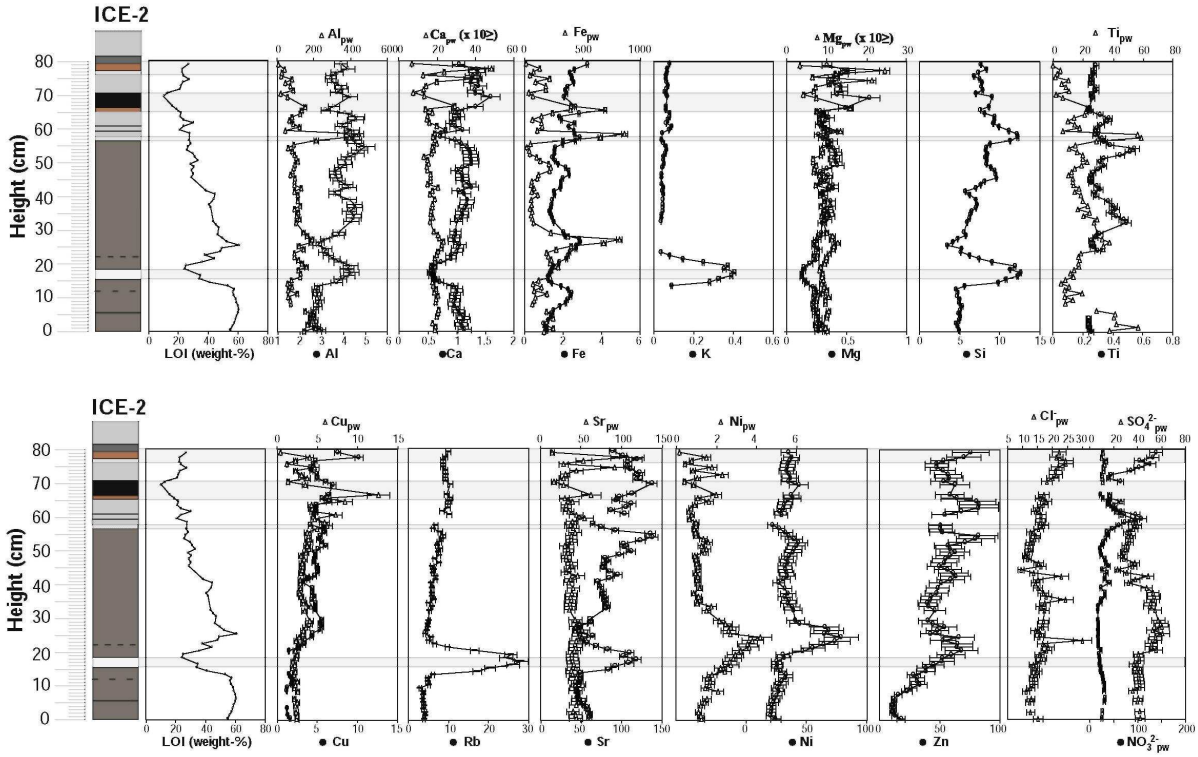

Table 3: *Concentration of cations and anions in peat pore-water of ICE 2 peat outcrop measured by HR-ICP-MS (MRAC, Tervuren) and Dionex 100 (ULB), respectively. DL: under the detection limit. A dash means that the pore-water volume necessary for analyses was not obtained.*

Depth (cm)	Al (µg/kg)	Ca (µg/kg)	Fe (µg/kg)	Mg (µg/kg)	Mn (µg/kg)	Na (µg/kg)	Ti (µg/kg)	Cd (µg/kg)	Cu (µg/kg)	Sr (µg/kg)	Pb (µg/kg)	Ni (µg/kg)	Zn (µg/kg)	cl^- (µg/kg)	NO_3^- (µg/kg	SO_4^{2-} (µg/kg)
0.5	146	18,883	172	10,033	2.252	14,823	38	0.050	2.414	44	0.958	1.240	5.13	14.45	25.07	42.15
1.5	208	19,232	251	9626	3.380	13,932	57	0.014	2.454	43	0.114	1.212	DL	-	-	-
2.5	164	17,620	177	8779	3.006	13,888	43	0.014	2.348	40	0.084	1.096	DL	12.10	25.85	41.63
3.5	-	-	-	-	-	-	-	-	-	-	-	-	-	-	-	-
4.5	177	19,688	248	10,002	1.830	15,135	41	0.054	2.268	44	0.044	1.230	139.2	-	-	-
5.5	197	20,481	246	10,094	2.652	14,750	42	0.014	2.488	47	0.106	1.398	DL	11.88	30.12	39.76
6.5	150	20,628	190	10,361	2.300	15,244	29	0.054	2.122	48	0.110	1.518	7.35	12.33	30.98	40.51
7.5	-	-	-	-	-	-	-	-	-	-	-	-	-	-	-	-
8.5	72	19,077	70	9570	1.024	14,439	9	0.028	2.538	43	0.626	2.060	37.5	10.84	29.27	36.03
9.5	69	19,460	87	9679	0.818	14,854	14	0.016	2.120	45	0.180	1.420	DL	12.13	30.47	41.68
10.5	56	20,353	95	10,509	1.312	14,900	8	0.012	2.244	47	0.776	1.656	DL	13.15	30.58	41.72
11.5	108	18,409	198	9027	2.498	13,689	20	0.012	2.474	42	0.180	1.682	DL	13.12	27.81	41.29
12.5	58	19,474	84	9988	1.096	14,231	8	DL	1.906	44	0.604	1.512	6.51	12.96	26.98	40.78
13.5	78	17,873	151	9327	2.612	14,337	11	DL	2.062	39	0.122	1.758	DL	13.53	25.29	40.64

14.5	55	17,575	75	8652	1.370	14,176	6	0.012	2.230	38	0.174	2.396	DL	14.18	21.96	39.27
15.5	75	19,185	124	9076	2.934	14,298	9	0.010	1.866	41	0.164	2.198	DL	13.52	22.71	40.37
16.5	123	17,780	223	8801	4.496	14,283	14	0.010	2.178	41	0.082	2.724	DL	13.00	19.57	36.80
17.5	125	17,351	214	8927	3.826	14,412	12	0.010	1.910	40	0.110	2.658	DL	15.08	20.61	41.40
18.5	115	16,534	233	8153	4.698	14,522	14	0.010	2.364	39	0.218	2.840	DL	15.39	20.34	41.21
19.5	158	16,839	294	8478	6.330	13,966	18	0.010	2.444	39	0.184	2.928	6.56	14.80	19.13	40.53
20.5	134	18,832	221	9456	2.420	14,786	17	0.012	2.214	42	0.120	3.210	DL	16.95	22.85	55.13
21.5	112	18,661	235	9779	3.124	14,762	18	0.010	2.600	44	0.152	3.612	5.88	17.55	18.16	51.18
22.5	90	19,872	205	9978	2.770	14,237	17	0.020	2.664	43	0.130	3.528	DL	15.85	18.32	51.34
23.5	90	20,305	193	10,595	1.154	14,154	19	0.010	2.306	44	DL	3.784	DL	27.93	18.26	54.29
24.5	143	22,200	274	11,532	2.334	13,446	34	0.010	2.710	48	0.124	4.168	DL	14.65	16.82	54.82
25.5	115	22,290	405	11,813	6.652	14,245	34	0.012	3.178	49	0.196	2.686	5.08	15.12	17.95	60.57
26.5	183	23,453	686	12,694	8.888	13,733	38	DL	3.232	51	0.252	2.592	DL	13.60	16.49	52.58
27.5	188	20,925	822	11,172	9.500	12,927	33	DL	3.592	44	0.188	2.716	DL	15.87	18.18	60.38
28.5	160	20,295	375	11,431	4.382	13,599	29	0.010	3.908	48	0.126	2.422	DL	15.86	17.65	59.06
29.5	142	18,226	231	9943	9.028	13,561	30	DL	4.008	43	1.036	2.120	DL	16.09	16.90	57.08
32.5	99	16,259	78	9049	0.580	12,257	28	0.032	3.378	36	0.018	1.498	DL	16.30	16.35	54.46
33.5	121	17,722	69	9343	1.932	12,884	30	0.042	4.154	37	0.336	1.748	17.03	15.30	17.25	50.01
34.5	104	16,679	58	8699	1.412	12,760	21	0.012	3.242	36	0.274	1.026	DL	16.48	22.50	50.54
35.5	114	16,820	69	9120	0.816	12,863	25	0.012	3.206	38	0.022	1.162	DL	22.83	23.36	52.91
36.5	91	17,475	49	9306	1.146	14,097	17	0.012	2.930	37	0.430	1.108	66.3	16.86	30.95	53.66
37.5	125	17,612	62	8488	1.138	13,798	24	0.010	2.802	38	0.192	0.854	14.7	16.07	31.78	52.61
39.0	111	18,677	60	9423	0.768	13,783	20	DL	2.830	41	0.024	1.160	7.98	14.43	22.88	47.28
40.5	111	16,090	115	8371	2.078	12,830	19	0.158	2.886	35	0.224	1.080	168	13.70	40.95	32.22
41.5	91	17,512	65	8918	1.702	13,151	15	0.022	2.896	37	1.318	1.014	17.30	14.47	30.45	37.94
42.5	129	20,438	83	10,278	1.808	14,683	18	0.018	3.924	46	0.256	1.076	6.29	21.53	31.53	48.52
43.5	93	15,042	61	7236	1.074	12,482	14	0.046	2.940	31	0.064	0.940	DL	13.12	35.69	30.94
44.5	91	16,495	65	8313	1.064	12,676	14	DL	3.068	36	0.104	1.076	75.63	9.27	25.12	23.15
45.5	94	16,628	109	8580	2.906	12,976	14	DL	3.138	39	0.096	1.060	7.53	15.27	38.90	35.66
46.5	70	16,569	123	8123	1.560	13,519	11	0.022	3.084	38	0.048	1.016	8.54	14.56	33.26	37.59
47.5	83	14,853	217	6707	3.350	12,130	13	0.048	3.326	32	0.172	0.980	DL	11.17	30.90	28.28
48.5	88	14,440	227	6914	2.984	11,778	15	0.020	2.962	32	DL	0.904	DL	10.67	23.81	26.34
39.0	111	18,677	60	9423	0.768	13,783	20	DL	2.830	41	0.024	1.160	7.98	14.43	22.88	47.28
49.5	95	15,452	211	7309	1.652	12,331	20	DL	3.576	34	0.026	1.396	DL	11.48	21.95	28.30
50.5	109	15,028	138	6551	1.774	12,367	23	DL	3.926	34	DL	1.496	17.41	11.77	21.39	29.66
51.5	100	13,073	107	6473	1.058	12,197	20	DL	3.674	30	0.084	1.234	11.03	11.72	25.34	29.88
52.5	93	17,130	48	8527	0.354	13,209	20	0.028	3.966	39	0.034	1.576	14.29	12.03	27.72	33.10
53.5	80	18,190	43	8995	0.268	14,346	17	DL	3.842	38	DL	1.348	DL	13.35	32.36	33.06
54.5	57	17,482	22	8572	0.506	14,744	11	DL	3.852	38	0.048	0.976	6.37	13.79	38.48	34.58
55.5	88	19,678	52	10,430	1.592	14,489	15	DL	3.744	43	0.212	0.944	DL	12.11	35.92	31.02
56.5	212	18,891	334	10,083	0.582	14,507	30	DL	4.932	40	0.020	0.876	DL	14.59	47.44	36.31
57.5	394	17,701	658	9570	1.202	14,835	59	DL	6.190	37	0.014	0.966	5.40	16.07	60.80	39.54
58.5	448	18,806	868	9878	1.776	15,252	57	DL	5.884	39	0.036	0.984	40.89	15.13	73.54	35.96
59.5	42	24,336	110	13,335	0.658	18,237	7	DL	4.662	55	DL	0.648	9.99	15.34	107.4	37.42
60.5	121	19,802	152	9496	0.680	16,717	18	0.024	7.276	44	DL	0.772	18.37	15.30	95.57	26.87
61.5	85	15,977	148	8642	0.878	14,799	15	DL	4.482	34	DL	0.596	DL	13.69	64.95	22.80
62.5	64	14,750	72	8027	0.972	15,175	10	DL	4.324	32	0.040	0.724	DL	14.38	51.00	20.57
63.5	78	14,996	147	8134	0.916	14,475	14	0.036	4.214	32	DL	0.916	10.27	15.93	38.16	19.27
64.5	125	17,465	243	9191	1.624	16,547	22	0.014	8.412	40	DL	1.612	9.59	16.80	38.75	25.98
65.5	132	13,813	400	7361	1.642	14,116	22	DL	5.974	30	0.018	1.068	DL	15.08	26.99	16.62
66.5	151	29,056	405	15,763	2.780	30,083	25	DL	12.624	63	0.060	1.972	52.78	16.19	21.91	16.56
69.5	52	13,206	75	7336	0.836	14,443	7	0.048	3.444	28	0.032	0.852	21.37	-	-	-
70.5	17	7528	39	4127	0.934	7321	2	DL	1.290	17	0.100	0.404	DL	17.08	64.21	10.83
71.5	86	12,960	184	6755	2.780	13,547	11	DL	3.702	28	0.246	1.034	DL	18.98	39.24	10.31
72.5	69	14,156	184	7137	2.114	14,412	9	DL	2.990	31	DL	2.270	9.39	19.89	44.37	10.31
73.5	43	19,885	98	10,593	1.152	16,698	6	DL	2.220	44	0.012	0.824	11.66	19.73	85.84	11.51
74.5	78	42,205	220	21,125	1.728	32,859	11	DL	4.664	92	DL	1.772	DL	20.40	102.4	11.55
75.5	18	12,689	46	6360	0.192	9422	2	DL	1.174	28	DL	0.440	DL	22.87	125.7	12.21
76.5	21	23,721	79	12,294	0.322	17,292	3	DL	2.242	53	DL	0.760	6.36	22.83	103.4	13.44
77.5	38	48,256	133	24,408	0.548	35,148	5	DL	4.036	107	DL	1.496	DL	19.96	131.7	9.71

Table 4: *(A) Calculation of metal release rate by H3 during the past 4 ka. (B) Calculation of concentration increase rates in the Fe peak above H3. See text for details.*

	Al	**Fe**	**K**	**Mg**	**Mn**	**Ca**	**Na**	**Si**	**Ti**	**Cu**	**Rb**	**Sr**	**Ni**	**Zn**
Mean concentration in fresh glass	3.89	4.86	0.39	0.35	0.15	2.56	1.58	30.9	0.30	-	-	-	-	-
Mean concentration in outcrop (16.5 cm height)	3.85	1.22	0.39	0.13	DL	0.57	DL	12.1	DL	DL	25.8	110.4	25.9	44.3
A. Release rate mg/kg/yr	0.10	9.10	1.03	0.55	-	4.97	-		46.79	-	-	-	-	-

Mean concentration in natural peat (24.5-27.5 cm height)	4.11	1.40	-	0.30	-	1.10	DL	6.35	0.41	4.41	6.55	79.0	34.9	44.1
Mean concentration in Fe peak (32.5-40.5 cm height)	2.47	2.8	0.05	0.3		1		4.35	0.27	4.77	5.38	47.8	66.8	50.6
B. Enrichment factor above H3	<0	100	-	0	-	<0	-	<0	<0	8.29	<0	<0	91.4	14.7

Fig. 4: *EDS elemental mapping of Veidivötn A.D. 1477 tephra showing compositional differences of glass shards (light grey in backscattered electron image and light green on the elemental mapping image) and the poorly crystalline Fe phases (dark grey on backscattered electron image and blue on the elemental mapping image).*

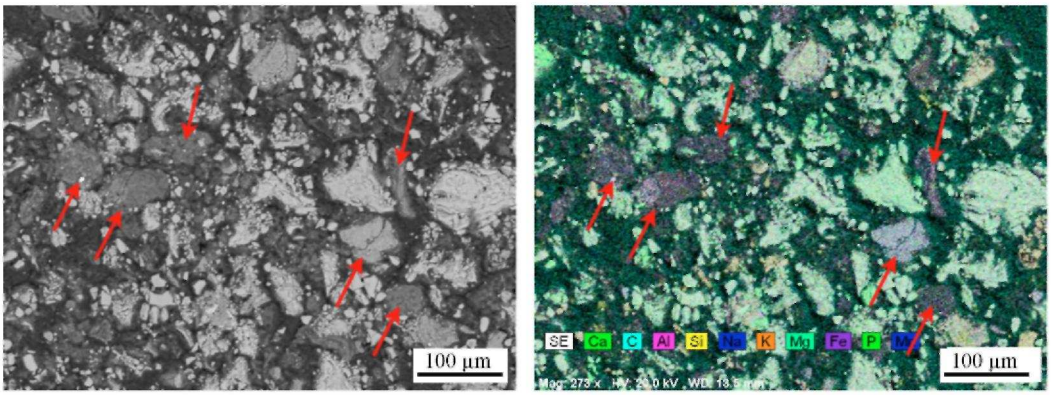

The behaviour of Ni seems dependent upon Fe and LOI. Above H3, there is a positive correlation between Ni, Fe and LOI, but also with Ni in pore water. $Nickel_{pw}$ and Fe_{pw} are moreover negatively correlated with a range of elements in the solid phase (i.e. Al, Ca, K, Mg, Si, Rb, Sr). These latter elements are related to H3 particles, which were scattered in the peat during burial and slightly disturbed by vegetation growth. This demonstrates that Ni does not come from the dissolution of H3 particles reworked just above the H3 layer. Rather it is suggested that Ni is transported by water, which percolates through the peat and is consequently blocked by H3 and is possibly scavenged by Fe oxyhydroxide. It is also in agreement with the positive correlation between Ni and Ca_{pw}, Fe_{pw}, Mg_{pw}, Mn_{pw}, Ti_{pw} and Sr_{pw} (Table 3). Below H3 (Table 2), Ni is again well correlated with Fe (r = 0.8), but also with Zn (r = 0.9). Though slightly enriched below H3, Ni is less concentrated than above. This feature leads to the hypothesis that Ni is more easily adsorbed on Fe-phases when organic matter is involved. This hypothesis is supported by previous studies, which showed that Ni was mainly scavenged by Fe oxyhydroxides (e.g. Xu et al., 2007; Gunsinger et al., 2006; Sterckeman et al., 2006; Dries et al., 2005; Hao et al., 2005; Stipp et al., 2002; Li et al., 2000). Nachtegaal and Sparks (2002) noted that this phenomenon was enhanced by the presence of humic acids. Grybos et al. (2007) also showed that Ni was adsorbed and/or co-precipitated on both Fe oxyhydroxides and organic matter. Nickel scavenging by amorphous Fe (III) oxides was recently experimentally demonstrated to occur at pH 6-7 (Xu et al., 2007).

EDS-SEM analyses of samples from the Fe rich layer above H3 suggest various compositions (Table 1). These particles are composed mainly of Si, Fe and Al. Iron content is variable. Moreover, one of the analysed particles has a low Fe content together with a low C content, suggesting the hypothesis that the behaviours of Fe and organic matter are linked. In thin section, a discontinuous cryptotephra occurs at this level (26 cm height, Fig. 1). However the Mg concentration profile is not affected by the scoria, compared to Mg concentrations in Veidivötn tephras. Likewise, Si displays lowest values (less than 4% at 26 cm height) of the profile, despite the presence of sparse basic scoria. It is, therefore, assumed that this discontinuous cryptotephra does not play a significant role on the geochemistry of the peat samples.

Below H3 (0.5-13.5 cm), LOI shows no relationship with chemical elements, for both the particles and the pore-water (Table 2). Therefore organic matter does not play a significant role in the control of Fe, Ni and Zn behaviour. Silicon also does not show any relationship with the other elements. It displays a poor positive relationship with K (r = 0.67), perhaps due to their association in glass particles from H3. Calcium, Sr, Ti and

Mg are correlated, but profiles show no variation in concentration. $Calcium_{pw}$, Mg_{pw}, Na_{pw}, Cu_{pw}, Sr_{pw}, Ni_{pw} display similar trends. $Aluminium_{pw}$, Mn_{pw}, Ti_{pw}, Fe_{pw} also show flat profiles, although with small point to point variation, but no significant relationship can be pointed out.

Fig. 5: *Fe oxihydroxide patches above H3. (A) General view showing large Fe patches in an organic mass. (B,C) Zoom views on large patches showing that even the organic mass is strongly oxidised. (D) SEM backscattered electron view of a patch of Fe oxihydroxide showing typical cracked structure.*

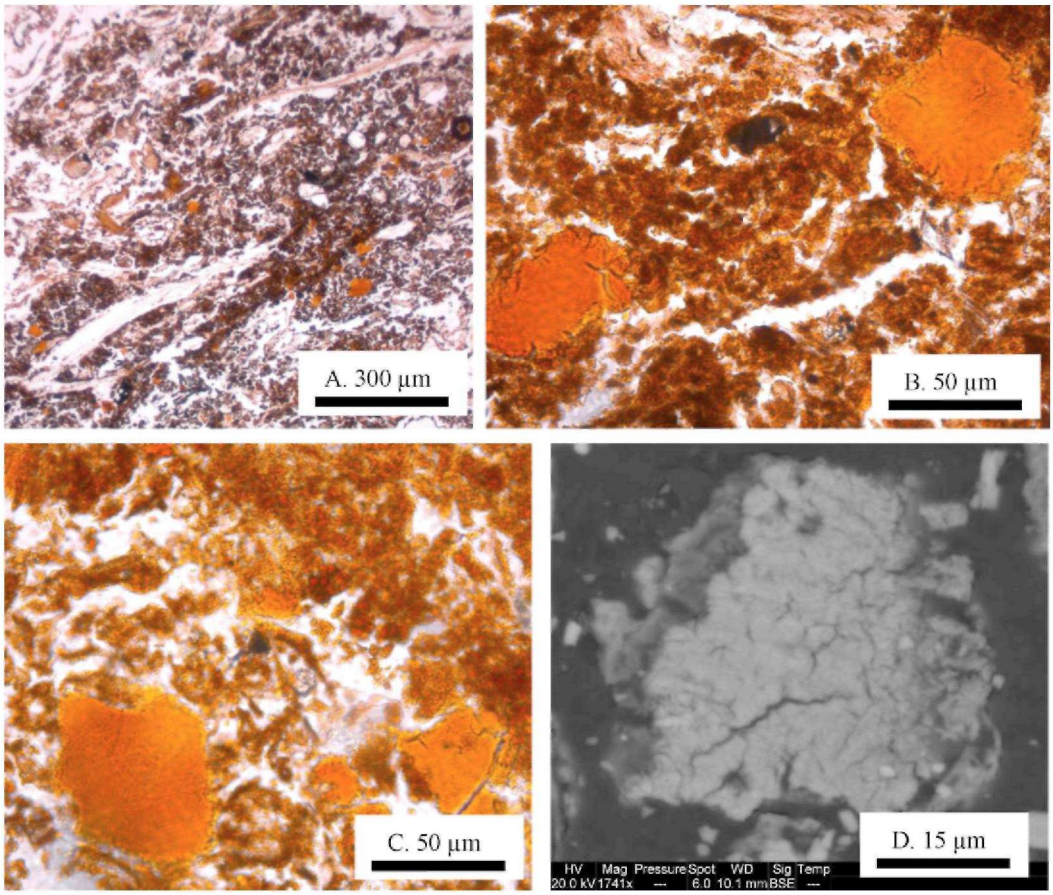

5.6. Barrier efficiency

From the Fe vs. depth profile, it appears that Fe concentrations are equal above and below H3. $Iron_{pw}$ is, however, less concentrated below H3 than above, which favours the hypothesis of a semi-efficient water barrier that allows partial percolation of water. The occurrence of Fe in poorly crystalline phases in the middle of H3 pumice proves that even if most of the water is effectively retained above H3, some may have penetrated it. Iron in poorly crystalline phases could thus precipitate within the tephra, or just below, during the early phase of this process. Moreover, the permeability would limit its percolation and facilitate (1) solution stagnation in tephra porosity, (2) amorphous clay neo-synthesis and (3) bacterial activity. Indeed, the porosity created by the tephra is a confined space for bacterial growth fed by the nutrient release from tephra weathering (K, P) and by the dissolved organics (i.e. fulvic acids) in percolating water (Lehman et al., 2004). The development of bacterial communities partially reduces the porosity and usually forms a protective thin film on particles or forms real oncolithes (see Figs. 3-5 in De Vleeschouwer et al., 2008). This progressive reduction of porosity will confine Fe precipitation above the H3 tephra.

6. Conclusions

The geochemical investigation of an Icelandic peat profile containing tephra suggests that the principal tephra characteristics affecting the peat geochemistry are the grain size, thickness and, to a lesser extent, the tephra

composition. A tephra having a sufficiently fine grain size (at least <20 µm) and a sufficient thickness (at least >1 cm) can act as a capillary barrier to water percolation and elemental diffusion, creating Fe-, Ni-(and Zn-) enriched layers above. Furthermore, the confined space at the surface of the porous tephra fragments causes higher concentrations of iron and trace metals to accumulate, allowing the formation of Fe-organic bearing minerals. For example, in the investigated peat column, the H3 tephra acts like a barrier, Fe precipitates in the form of a Fe-amorphous phase above the tephra and scavenges Ni. Conversely, the coarser but thinner tephras encountered in the same outcrop do not act in the same way as the H3 deposit. The tephra composition seems to play a role in terms of elemental leaching. Basic tephras are more easily leached than acidic ones. However, this leaching can be slowed down by protective films formed around grains. Therefore, the amount of elements released from leaching is low compared to the concentrations encountered in such mineral-rich peat. More research should be directed to other peat bogs containing tephra deposits in order to precisely determine the minimum grain size/thickness ratio necessary to form an active barrier.

Fig. 6: *Example of significant correlation in samples above H3 tephra.*

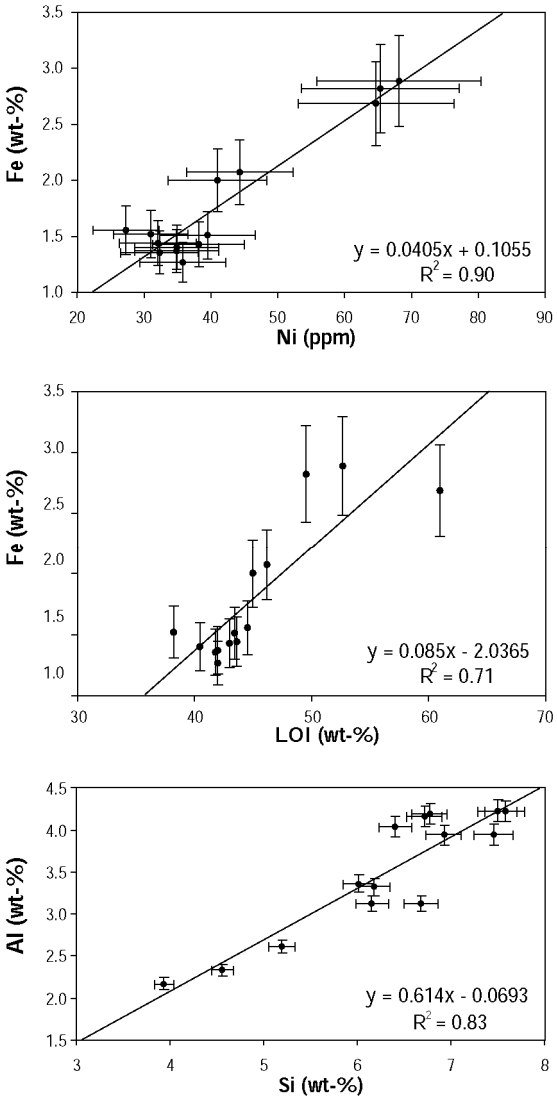

Acknowledgements

Xavier Boës and Jean-Paul Cullus were of great help in the thin section preparation. We also warmly thank Jacques Navez and Laurence Monin (MRAC Tervuren), and Philippe Recourt (UMR-PBDS, Lille, France) for their assistance with pore-water analysis and SEM-EDS analysis, respectively. Guy Bologne and Sophie

Leclercq (LJRPGE, LJLg) were also very helpful during the calibration of the XRF. We are grateful to Maria Gehrels, Dmitri Mauquoy, Gunnar Mallon and Domenik Wolff-Boenisch for their comments and corrections to the English. We would like to finally acknowledge Morgan Jones, one anonymous reviewer and editor Ron Fuge for their high quality reviews and comments. The impregnation laboratory at LJRAP has been developed and optimised thanks to University fund Nr R.CERA.0438. This work is also supported by the French program IPROCI, funded by the Institut Paul Emile Victor (Iceland field mission and SEM-EDS analysis) and by NSRF (Belgian Scientific Research Foundation) credits. François De Vleeschouwer is supported by a FRIA fellowship.

Appendix A

Certified and measured values used for trace element XRF calibration. Concentrations in mg/kg. Accuracies and detection limits (DL) are also reported. Note that generally, accuracy decreases with the decrease of certified value concentrations. This feature is enhanced when reaching the detection limit.

		Recom	**Measured**	**Error (%)**	**Recom**	**Measured**	**Error (%)**
		Cu			**Pb**		
CLB1	Coal	10	35	248	5.1	9	76.5
1632b	Coal	-	-	-	-	-	-
NIES2	Pond sediment	210	206	2.1	105	94.8	9.7
NIES7	Tea leaves	-	-	-	-	-	-
NIES8	Veh. part, exhaust	67	65.9	1.6	219	225.6	3.0
JSD-2	Sediment	1114	1115	0.04	151	147	2.6
JSD3	Sediment	426	419.1	1.6	82	79.8	2.7
SGR	Sediment	66	52.2	20.9	38	36.2	4.7
BCR 482	Lichen	-	-	-	40.9	45.4	11.0
BCR 100	Beach leaves	-	-	-	16.3	18.2	11.7
Mean				5			6
Median				5			6
		Rb			**Ni**		
CLB1	Coal	5.2	5.8	11.5	18	23.7	31.7
1632b	Coal	5.05	5.4	6.9	6.1	9.4	54.1
NIES2	Pond sediment	42	39.6	5.7	40	37.2	7.0
NIES7	Tea leaves	-	-	-	6.5	3.6	44.6
NIES8	Veh. part, exhaust				18.5	13.3	28.1
JSD-2	Sediment	27	25.9	4.1	94	93.5	0.5
JSD3	Sediment	285	287	0.7	19.6	25.3	29.1
SGR	Sediment	83	76.2	8.2	29	25.8	11.0
BCR 482	Lichen	-	-	-	2.47	1.9	23.1
BCR 100	beach leaves	-	-	-	-	-	-
Mean				6			19
Median				6			19
		Sr			**Zn**		
CLB1	Coal	-	-	-	48	73	52.1
1632b	Coal	-	-	-	11.89	20.5	72.4
NIES2	Pond sediment	110	109.4	0.5	343	323.9	5.6
NIES7	Tea leaves	-	-	-	33	16	51.5
NIES8	Veh. part, exhaust	89	90.1	1.2	1040	1173.6	12.8
JSD-2	Sediment	202	228.8	13.3	2070	1992.8	3.7
JSD3	Sediment	60	57.6	4.0	139	123	11.5
SGR	Sediment	420	403.2	4.0	74	54.9	25.8
BCR 482	Lichen	-	-	-	100.6	128.7	27.9
BCR 100	beach leaves	-	-	-	-	-	-
Mean				5			20
Median				5			20

Published in: Applied Geochemistry (2008), vol.23, iss.12, pp. 3819-3839
Status: Postprint (Author's version)

Appendix B

Analyses and statistics of five peat aliquots (PIS a-e), artificial mix (PISAM 0) and its progressive dilutions (PI-SAM 1-5) measured by ICP-AES. Concentrations are given in wt%. Mean, standard deviation and reproducibility of PI-SAM samples are based on six runs. Medians are calculated from PISAM 1 to PISAM 4. PISAM 0 is not taken into account because it is not used in calibration lines. PISAM 5 is not used because it is too low. Values in bold were not taken into account for the calculation of median accuracy.

	Al	Ca	Fe	K	Mg	Mn	Na	Si	Ti
Peat									
PIS a	0.0464	0.5009	0.0493	0.0173	0.0478	0.0006	0.0102	0.0003	0.0029
PIS b	0.0436	0.4687	0.0469	0.0162	0.0448	0.0006	0.0096	0.0007	0.0026
PIS c	0.0462	0.5295	0.0496	0.0173	0.0481	0.0006	0.0103	0.0007	0.0029
PIS d	0.0440	0.4691	0.0503	0.0167	0.0456	0.0006	0.0099	-	0.0028
PIS e	0.0438	0.4777	0.0505	0.0167	0.0453	0.0006	0.0096	-	0.0029
Mean	0.0448	0.4892	0.0493	0.0168	0.0464	0.0006	0.0099	-	0.0028
Stdev	0.0014	0.0261	0.0014	0.0005	0.0015	0.0000	0.0003	-	0.0001
Reprod (%)	97	95	97	97	97	97	97	-	95
Artificial mix									
Reference values									
PISAM 0	6.172	1.819	8.668	0.342	0.622	0.047	2.189	19.002	0.526
PISAM 1	4.896	1.291	5.384	0.520	0.396	0.032	1.510	12.666	0.363
PISAM 2	3.368	1.071	3.767	0.207	0.308	0.020	1.006	8.441	0.228
PISAM 3	2.131	0.814	2.404	0.112	0.200	0.012	0.837	5.583	0.127
PISAM 4	1.434	0.724	1.703	0.117	0.146	0.008	0.336	3.652	0.103
PISAM 5	0.670	0.543	0.731	0.068	0.092	0.004	0.160	1.699	0.051
Mean concentration									
PISAM 0	11.785	1.499	7.163	1.070	0.597	0.040	4.254	22.560	0.444
PISAM 1	4.979	1.455	5.916	0.547	0.427	0.031	1.571	12.904	0.385
PISAM 2	3.302	0.958	4.332	0.286	0.268	0.018	0.815	8.043	0.291
PISAM 3	1.801	0.786	2.942	0.081	0.185	0.011	0.289	5.411	0.111
PISAM 4	1.371	0.577	1.502	0.129	0.145	0.015	0.249	3.601	0.083
PISAM 5	1.202	0.800	0.105	0.115	0.122	• 0.002	0.228	2.217	0.051
Standard deviation									
PISAM 0	0.8581	0.2019	0.7346	0.0731	0.0357	0.0003	0.2946	1.6007	0.0273
PISAM 1	0.0298	0.0216	0.0539	0.0375	0.0032	0.0008	0.0137	0.0194	0.0080
PISAM 2	0.0187	0.0173	0.0751	0.0212	0.0020	0.0019	0.0282	0.0370	0.0034
PISAM 3	0.0250	0.0098	0.0304	0.0241	0.0008	0.0011	0.0122	0.0507	0.0047
PISAM 4	0.0139	0.0092	0.0494	0.0240	0.0002	0.0006	0.0127	0.0184	0.0022
PISAM 5	0.0057	0.0178	0.0130	0.0040	0.0008	0.0008	0.0040	0.0277	0.0025
Median (PISAM 1-4)	0.0219	0.0136	0.0517	0.0241	0.0014	0.0010	0.0132	0.0282	0.0041
Reproducibility									
PISAM 0	93	87	90	93	94	99	93	93	94
PISAM 1	99	99	99	93	99	97	99	100	98
PISAM 2	99	98	98	93	99	90	97	100	99
PISAM 3	99	99	99	70	100	90	96	99	96
PISAM 4	99	98	97	81	100	96	95	99	97
PISAM 5	100	98	88	97	99	142	98	99	95
Median (PISAM 1-4)	99	99	99	87	100	93	97	100	98
Accuracy									
PISAM 0	91	18	17	213	4	14	94	19	16
PISAM 1	2	13	10	5	8	5	4	2	6
PISAM 2	2	11	15	38	13	8	19	5	28
PISAM 3	15	3	22	28	8	8	65	3	13
PISAM 4	4	20	12	11	1	83	26	1	20
PISAM 5	79	47	86	68	33	155	43	30	1
Median (PISAM 1-4)	3	12	14	20	7	8	23	3	17
Mean DL									
PISAM 1	0.9580	0.0434	0.1355	0.0322	0.1809	0.0412	1.3662	2.6116	0.5692
PISAM 2	0.7744	0.0449	0.1211	0.0344	0.1399	0.0432	1.0561	1.6954	0.4531
PISAM 3	0.6305	0.0471	0.1040	0.0367	0.1161	0.0391	0.8692	1.1785	0.2213

PISAM 4	0.5765	0.0503	0.0867	0.0451	0.1054	0.0457	0.7949	0.8191	0.2288
PISAM 5	0.5613	0.0667	0.0755	0.0574	0.1049	0.0458	0.8326	0.5586	0.1701
Median (PISAM 1-4)	0.7025	0.0460	0.1126	0.0356	0.1280	0.0422	0.9627	1.4370	0.3410

Appendix C

Autocorrelation performed above H3 tephra (25.5-41.5 cm height). Positive correlation >0.8 are in bold, negative correlation r < 0.8 are in italics.

	LOI	Al	Ca	Fe	K	Mg	Si	Ti	Cu	Rb	Sr	Ni	Zn	Al_{pw}	Ca_{pw}	Fe_{pw}	Mg_{pw}	Mn_{pw}	Na_{pw}	Ti_{pw}	Cu_{pw}	Sr_{pw}	Pb_{pw}	Ni_{pw}	Zn_{pw}	Cl^-_{pw}	$NO_3^-{}_{pw}$
LOI	1																										
Al	*-0.905*	1																									
Ca	-0.465	0.583	1																								
Fe	**0.857**	*-0.931*	-0.718	1																							
K	-0.730	0.787	**0.833**	*-0.897*	1																						
Mg	*-0.853*	**0.924**	0.788	*-0.921*	**0.849**	1																					
Si	*-0.938*	**0.917**	0.709	*-0.917*	**0.838**	**0.938**	1																				
Ti	-0.677	**0.879**	0.410	-0.789	0.708	0.709	0.661	1																			
Cu	0.184	-0.216	-0.738	0.519	-0.721	-0.379	-0.374	-0.183	1																		
Rb	*-0.843*	0.791	0.683	*-0.860*	**0.856**	**0.839**	**0.901**	0.591	-0.500	1																	
Sr	*-0.848*	**0.952**	0.622	*-0.978*	**0.869**	**0.889**	**0.873**	**0.880**	-0.438	**0.810**	1																
Ni	**0.845**	*-0.837*	-0.704	**0.951**	*-0.833*	*-0.856*	*-0.915*	-0.611	0.557	*-0.830*	*-0.888*	1															
Zn	0.138	-0.384	-0.061	0.356	-0.049	-0.284	-0.116	-0.430	-0.142	-0.043	-0.381	0.246	1														
Al_{pw}	0.411	-0.649	-0.714	0.793	-0.768	-0.636	-0.573	-0.684	0.668	-0.524	-0.769	0.731	0.435	1													
Ca_{pw}	**0.832**	*-0.817*	-0.526	**0.909**	*-0.809*	-0.758	*-0.809*	-0.707	0.508	-0.764	*-0.906*	**0.906**	0.229	0.724	1												
Fe_{pw}	0.692	*-0.844*	-0.739	**0.951**	*-0.830*	*-0.834*	-0.797	-0.760	0.575	-0.737	*-0.916*	**0.910**	0.485	**0.895**	**0.841**	1											
Mg_{pw}	**0.816**	*-0.819*	-0.693	**0.913**	*-0.880*	*-0.833*	*-0.846*	-0.692	0.591	*-0.800*	*-0.893*	**0.904**	0.146	0.737	**0.962**	**0.854**	1										
Mn_{pw}	0.678	*-0.823*	-0.754	**0.909**	*-0.915*	*-0.824*	*-0.804*	-0.767	0.639	-0.752	*-0.906*	**0.817**	0.205	**0.815**	0.763	**0.871**	0.787	1									
Na_{pw}	0.408	-0.291	0.206	0.309	-0.296	-0.146	-0.186	-0.411	0.103	-0.227	-0.425	0.254	-0.078	0.101	0.553	0.165	0.434	0.272	1								
Ti_{pw}	0.709	-0.710	-0.796	**0.830**	*-0.822*	*-0.801*	*-0.850*	-0.450	0.614	-0.717	-0.740	**0.890**	0.071	0.733	0.782	0.770	**0.820**	0.775	0.087	1							
Cu_{pw}	0.069	-0.094	-0.682	0.237	-0.529	-0.294	-0.275	-0.020	0.649	-0.280	-0.131	0.237	-0.374	0.409	0.147	0.253	0.299	0.420	-0.253	0.516	1						
Sr_{pw}	0.785	-0.782	-0.584	**0.861**	*-0.876*	-0.747	-0.780	-0.730	0.565	-0.765	*-0.876*	**0.828**	0.089	0.711	**0.955**	0.771	**0.961**	0.763	0.573	0.767	0.246	1					
Pb_{pw}	-0.029	-0.048	-0.220	0.100	-0.321	-0.112	-0.075	-0.131	0.368	-0.130	-0.147	-0.022	-0.397	0.107	-0.015	0.011	0.020	0.461	0.232	0.092	0.430	0.075	1				
Ni_{pw}	**0.802**	*-0.826*	*-0.834*	**0.923**	*-0.950*	*-0.897*	*-0.888*	-0.664	0.644	*-0.831*	*-0.867*	**0.893**	0.131	0.757	**0.849**	**0.867**	**0.919**	**0.870**	0.230	**0.881**	0.547	**0.857**	0.162	1			
Zn_{pw}	-0.167	0.002	0.403	-0.261	0.429	0.091	0.257	-0.113	-0.738	0.330	0.162	-0.443	0.329	-0.321	-0.386	-0.260	-0.405	-0.259	-0.077	-0.530	-0.387	-0.437	0.031	-0.385	1		
Cl^-_{pw}	-0.351	0.389	0.087	-0.396	0.258	0.370	0.293	0.309	-0.016	0.434	0.408	-0.237	-0.396	-0.242	-0.371	-0.295	-0.285	-0.311	-0.245	-0.194	0.023	-0.289	-0.134	-0.288	-0.283	1	
$NO_3^-{}_{pw}$	-0.397	0.267	0.715	-0.478	0.650	0.437	0.537	0.034	-0.788	0.559	0.354	-0.600	0.299	-0.434	-0.508	-0.438	-0.609	-0.477	0.052	-0.744	-0.670	-0.557	-0.087	-0.681	**0.844**	-0.040	1
$SO_4^{2-}{}_{pw}$	0.384	-0.230	-0.546	0.476	-0.653	-0.369	-0.440	-0.128	0.776	-0.508	-0.393	0.601	-0.260	0.384	0.516	0.454	0.572	0.469	0.293	0.568	0.424	0.573	0.127	0.608	*-0.809*	0.255	-0.736

Appendix D

Autocorrelation performed below H3 tephra (0.5-13.5 cm depth). Positive correlation >0.8 are in bold, negative correlation *r* < 0.8 are in italics.

	LOI	Al	Ca	Fe	K	Mg	Si	Ti	Cu	Rb	Sr	Ni	Zn	Al_{pw}	Ca_{pw}	Fe_{pw}	Mg_{pw}	Mn_{pw}	Na_{pw}	Ti_{pw}	Cu_{pw}	Sr_{pw}	Pb_{pw}	Ni_{pw}	Zn_{pw}	Cl^-_{pw}	$NO_3^-{}_{pw}$	$SO_4^{2-}{}_{pw}$
LOI	1																											
Al	-0.534	1																										
Ca	-0.008	-0.302	1																									
Fe	-0.037	0.361	-0.786	1																								
K	-0.629	0.231	-0.418	0.102	1																							
Mg	0.012	-0.275	**0.967**	-0.656	-0.553	1																						
Si	-0.073	0.235	-0.364	0.020	0.667	-0.513	1																					
Ti	-0.222	-0.156	**0.888**	*-0.800*	-0.207	**0.844**	-0.234	1																				
Cu	-0.690	0.610	-0.174	0.530	0.202	-0.080	-0.213	-0.118	1																			
Rb	-0.734	0.120	-0.354	0.320	0.718	-0.355	0.122	-0.184	0.480	1																		
Sr	-0.454	-0.060	**0.812**	-0.716	-0.106	0.795	-0.369	**0.900**	0.091	0.063	1																	
Ni	-0.431	0.451	-0.719	0.799	0.507	-0.684	0.158	-0.688	0.614	0.665	-0.466	1																
Zn	-0.441	0.517	-0.645	**0.894**	0.282	-0.534	-0.078	-0.608	0.784	0.576	-0.415	**0.893**	1															
Al_{pw}	-0.011	-0.338	0.468	-0.527	-0.116	0.461	-0.243	0.372	-0.322	-0.099	0.381	-0.461	-0.451	1														
Ca_{pw}	-0.179	-0.003	-0.075	0.169	0.056	-0.023	-0.286	-0.153	0.168	0.206	-0.108	0.191	0.275	0.658	1													
Fe_{pw}	-0.130	-0.310	0.367	-0.367	0.036	0.374	-0.146	0.260	-0.202	0.101	0.307	-0.280	-0.278	**0.954**	0.694	1												
Mg_{pw}	-0.214	0.025	-0.070	0.166	0.078	-0.023	-0.272	-0.140	0.191	0.230	-0.092	0.210	0.289	0.644	**0.998**	0.681	1											
Mn_{pw}	-0.381	-0.142	0.238	-0.364	0.225	0.239	-0.178	0.234	-0.053	0.312	0.398	-0.141	-0.165	**0.867**	0.662	**0.896**	0.655	1										
Na_{pw}	-0.222	0.032	-0.073	0.152	0.103	-0.032	-0.247	-0.126	0.169	0.228	-0.091	0.199	0.273	0.652	**0.996**	0.689	**0.997**	0.668	1									
Ti_{pw}	-0.054	-0.291	0.594	-0.650	-0.180	0.589	-0.281	0.543	-0.323	-0.161	0.552	-0.580	-0.542	**0.970**	0.521	**0.892**	0.510	**0.825**	0.517	1								
Cu_{pw}	-0.234	0.030	-0.014	0.092	0.035	0.038	-0.320	-0.053	0.174	0.200	0.001	0.111	0.211	0.718	**0.966**	0.739	**0.961**	0.739	**0.968**	0.598	1							
Sr_{pw}	-0.166	0.010	-0.069	0.173	0.030	-0.014	-0.297	-0.157	0.170	0.183	-0.114	0.183	0.275	0.654	**0.999**	0.686	**0.997**	0.652	**0.994**	0.517	**0.965**	1						
Pb_{pw}	-0.324	0.499	-0.047	0.309	-0.142	-0.002	-0.354	-0.071	0.587	0.176	0.018	0.389	0.508	-0.093	0.381	-0.129	0.417	-0.059	0.382	-0.117	0.369	0.396	1					
Ni_{pw}	-0.246	0.143	-0.387	0.450	0.236	-0.336	-0.133	-0.405	0.352	0.377	-0.341	0.476	0.519	0.368	**0.899**	0.449	**0.898**	0.487	**0.900**	0.188	**0.882**	**0.895**	0.443	1				
Zn_{pw}	0.248	-0.371	0.258	-0.126	-0.108	0.236	0.151	0.296	-0.328	-0.101	-0.002	-0.247	-0.266	0.264	0.175	0.299	0.178	-0.034	0.192	0.228	0.164	0.161	-0.099	0.095	1			
Cl^-_{pw}	-0.288	0.332	-0.359	0.398	0.216	-0.353	-0.182	-0.469	0.351	0.316	-0.303	0.565	0.555	0.086	0.621	0.133	0.630	0.304	0.636	-0.055	0.588	0.635	0.534	0.704	-0.382	1		
$NO_3^-{}_{pw}$	-0.086	0.224	-0.431	0.450	0.110	-0.412	-0.205	-0.569	0.252	0.182	-0.455	0.498	0.515	0.086	0.639	0.110	0.637	0.243	0.642	-0.078	0.597	0.655	0.470	0.735	-0.356	**0.968**	1	
$SO_4^{2-}{}_{pw}$	-0.220	0.284	-0.373	0.398	0.175	-0.363	-0.209	-0.487	0.299	0.265	-0.337	0.527	0.528	0.097	0.628	0.132	0.632	0.297	0.640	-0.047	0.594	0.643	0.491	0.705	-0.382	**0.995**	**0.984**	1

Published in: Applied Geochemistry (2008), vol.23, iss.12, pp. 3819-3839
Status: Postprint (Author's version)

Appendix E

Autocorrelation performed below H1 158 tephra (41.5-58.5 cm depth). Positive correlation >0.8 are in bold, negative correlation $r < 0.8$ are in italics.

	Al	Ca	Fe	K	Mg	Si	Ti	Cu	Rb	Sr	Ni	Zn	Al_{pw}	Ca_{pw}	Fe_{pw}	Mg_{pw}	Mn_{pw}	Na_{pw}	Ti_{pw}	Cu_{pw}	Sr_{pw}	Pb_{pw}	Ni_{pw}	Zn_{pw}	Cl^-_{pw}	$NO_3^-{}_{pw}$	$SO_4^{2-}{}_{pw}$
Al	1																										
Ca	0.166	1																									
Fe	-0.168	*-0.837*	1																								
K	0.488	0.550	-0.578	1																							
Mg	0.527	**0.826**	-0.620	0.662	1																						
Si	0.093	-0.752	**0.846**	-0.366	-0.402	1																					
Ti	**0.904**	0.318	-0.401	0.582	0.556	-0.111	1																				
Cu	0.300	0.658	-0.438	0.149	0.634	-0.401	0.330	1																			
Rb	0.265	0.633	-0.485	0.178	0.590	-0.493	0.412	**0.870**	1																		
Sr	0.462	**0.801**	-0.722	0.484	0.777	-0.592	0.673	0.768	**0.883**	1																	
Ni	0.122	**0.865**	-0.703	0.296	0.716	-0.651	0.314	**0.858**	**0.889**	**0.894**	1																
Zn	0.388	0.720	-0.623	0.291	0.667	-0.613	0.575	0.783	**0.909**	**0.953**	**0.867**	1															
Al_{pw}	0.070	*-0.834*	0.712	-0.303	-0.496	0.773	-0.178	-0.715	-0.738	-0.760	*-0.866*	-0.748	1														
Ca_{pw}	0.404	-0.301	0.268	0.172	-0.136	0.168	0.244	-0.220	-0.221	-0.184	-0.410	-0.150	0.341	1													
Fe_{pw}	-0.069	*-0.853*	0.768	-0.347	-0.560	**0.822**	-0.261	-0.767	-0.755	-0.787	*-0.865*	-0.799	**0.956**	0.182	1												
Mg_{pw}	0.386	-0.430	0.366	0.092	-0.225	0.280	0.185	-0.229	-0.284	-0.287	-0.492	-0.245	0.446	**0.966**	0.278	1											
Mn_{pw}	-0.722	-0.190	0.249	-0.367	-0.519	0.042	-0.657	-0.255	-0.192	-0.349	-0.140	-0.342	-0.043	-0.286	0.141	-0.306	1										
Na_{pw}	0.569	-0.464	0.381	0.163	-0.153	0.419	0.388	-0.326	-0.306	-0.244	-0.551	-0.231	0.557	**0.876**	0.405	**0.887**	-0.431	1									
Ti_{pw}	0.143	-0.768	0.635	-0.267	-0.381	0.755	-0.091	-0.626	-0.623	-0.645	-0.756	-0.652	**0.978**	0.272	**0.927**	0.375	-0.112	0.508	1								
Cu_{pw}	0.415	-0.674	0.597	-0.139	-0.216	0.776	0.166	-0.456	-0.482	-0.467	-0.660	-0.493	**0.904**	0.439	**0.825**	0.512	-0.278	0.691	**0.933**	1							
Sr_{pw}	0.319	-0.153	0.171	0.239	-0.048	0.095	0.181	-0.123	-0.128	-0.108	-0.268	-0.101	0.207	**0.952**	0.053	**0.903**	-0.202	0.787	0.144	0.322	1						
Pb_{pw}	-0.342	-0.076	-0.266	0.013	-0.306	-0.543	-0.219	-0.125	0.003	-0.065	-0.031	0.028	-0.148	0.164	-0.203	0.164	0.129	-0.032	-0.181	-0.292	0.140	1					
Ni_{pw}	0.178	0.568	-0.612	0.398	0.629	-0.277	0.333	0.212	0.274	0.496	0.509	0.338	-0.246	-0.226	-0.276	-0.323	-0.300	-0.270	-0.097	-0.064	-0.113	-0.168	1				
Zn_{pw}	-0.273	-0.193	-0.016	-0.369	-0.358	0.018	-0.298	-0.362	-0.421	-0.396	-0.329	-0.362	0.212	0.033	0.161	0.062	-0.113	-0.002	0.160	0.046	0.023	0.072	0.054	1			
Cl^-_{pw}	0.136	-0.190	0.250	0.160	-0.052	0.091	-0.034	-0.262	-0.221	-0.211	-0.315	-0.133	0.353	0.644	0.215	0.616	-0.027	0.638	0.290	0.367	0.687	0.171	-0.233	-0.237	1		
$NO_3^-{}_{pw}$	0.173	*-0.848*	0.728	-0.201	-0.546	0.766	-0.046	-0.673	-0.723	-0.721	*-0.901*	-0.685	**0.887**	0.495	**0.831**	0.599	-0.091	0.733	**0.813**	**0.809**	0.351	-0.114	-0.464	0.092	0.441	1	
$SO_4^{2-}{}_{pw}$	0.171	-0.208	0.222	0.201	-0.045	0.081	0.036	-0.225	-0.152	-0.160	-0.272	-0.085	0.333	0.662	0.187	0.640	-0.116	0.668	0.289	0.382	0.709	0.258	-0.181	-0.265	**0.972**	0.433	1

References

Blodau, C, Moore, T.R., 2002. Macroporosity affects water movement and pore water sampling in peat soils. Soil Sci. 167, 98-109.

Boës, X., Fagel, N., 2005. Impregnation method for detecting annual laminations in sediment cores: an overview. Sed. Geol. 179,185-194.

Boygle, J., 1999. Variability of tephra in lake and catchment sediments, Svinavatn, Iceland. Global Planet. Change 21, 129-149.

Carboa, P., Kroma, M.D., Homokya, W.B., Benninga, L.G., Herutb, B., 2005. Impact of atmospheric deposition on N and P geochemistry in the southeastern Levantine basin. Deep Sea Res. Part II: Trop. Stud. Oceanogr. 52, 3041-3053.

Cornell, R.M., Giovanoli, R., Schneider, W., 1989. Review of the hydrolysis of iron (III) and the crystallization of amorphous iron (III) hydroxide hydrate. J. Chem. Technol. Biotechnol. 46, 115-134.

Daniels, R.E., Pearson, M.C., Ryden, B.E., 1977. A thermal-electric method for measuring lateral movement of water in peat. J. Ecol. 65, 839-846.

De Vleeschouwer, F., Van Vliet-Lanoë, B., Fagel, N., Richter, T.O., Boës, X., 2008. High resolution petrography on resin-impregnated Holocene peat columns containing tephras. Principle, applications and perspectives. Quatern. Int. 178, 54-67.

Dries, J., Bastiaens, L, Springael, D., Kuypers, S., Agathos, S.N., Diels, L, 2005. Effect of humic acids on heavy metal removal by zero-valent iron in batch and continuous flow column systems. Water Res. 39, 3531-3540.

Eirfksson, J., Larsen, G., Knudsen, K., Heinemeier, J., Sfmonarson, L.A., 2004. Marine reservoir age variability and water mass distribution in the Iceland Sea. Quatern. Sci. Rev. 23, 2247-2268.

Flaathen, T.K., Gislason, S.R., 2007. The effect of volcanic eruptions on the chemistry of surface waters: the 1991 and 2000 eruptions of Mt. Hekla, Iceland. J. Volcan. Geotherm. Res. 164, 293-316.

Gislason, S.R., Oelkers, E., 2003. Mechanism, rates, and consequences of basaltic glass dissolution: II. An experimental study of the dissolution rates of basaltic glass as a function of pH and temperature. Geochim. Cosmochim. Acta 67, 3817-3832.

Glasauer, S., Langley, S., Beveridge, T.J., 2002. Intracellular iron minerals in a dissimilatory iron-reducing bacterium. Science 295, 117-119.

Grybos, M., Davranche, M., Gruau, G., Petitjean, P., 2007. Is trace metal release in wetland soils controlled by organic matter mobility or Fe-oxyhydroxides reduction? J. Colloid Interface Sci. 314, 490-501.

Gunsinger, M.R., Ptacek, C.J., Blowes, D.W., Jambor, J.L., Moncur, M.C., 2006. Mechanisms controlling acid neutralization and metal mobility within a Ni-rich tailings impoundment. Appl. Geochem. 21, 1301-1321.

Haeckel, M., van Beusekom, J., Wieser, M.G., König, I., 2001. The impact of the Mount Pinatubo tephra fallout on the geochemical environment of the deep-sea sediments in the South China Sea. Earth Planet. Sci.Lett. 193, 151-166.

Hao, Z.-W., Xu, X.-H., Jin, J., He, P., Liu, Y., Wang, D.-H., 2005. Simultaneous removal of nitrate and heavy metals by iron metal. J. Zhejiang Univ. Sci. 6, 307-310.

Hodder, A.P.W., De Lange, P.J., Lowe, D.J., 1991. Dissolution and depletion of ferromagnesian minerals from Holocene tephra layers in an acid bog. New Zealand, and implications for tephra correlation. J. Quatern. Sci. 6, 195-208.

Holmes, J., Hall, V., Wilson, P., 1999. Volcanoes and peat bogs. Geology Today, March-April, pp. 61-63.

Hotes, S., Poschold, P., Takahashi, H., Grootjans, A.P., Adema, E., 2004. Effects of tephra deposition on mire vegetation: a field experiment in Hokkaido, Japan. J. Ecol. 92, 624-634.

Jin, Z., Li, F., Cao, J., Wang, S., Yu, J., 2006. Geochemistry of Daihai Lake sediments. Inner Mongolia, north China: implications for provenance, sedimentary sorting, and catchment weathering. Geomorphology 80, 147-163.

Johnson, K.R., Hub, C, Belshawa, N.S., Hendersona, G.M., 2006. Seasonal trace-element and stable-isotope variations in a Chinese speleothem: The potential for high-resolution paleomonsoon reconstruction. Earth Planet. Sci. Lett. 244, 394-407.

Lacasse, C, 2001. Influence of climate variability on the atmospheric transport of Icelandic tephra in the subpolar North Atlantic. Global Planet. Change 29, 31-55.

Larsen, G., Thorarinsson, S., 1977. H_4 and other acid Hekla tephra layers. Jökull 27, 27-46.

Larsen, G., Dugmore, A., Newton, A., 1999. Geochemistry of historical-age silicic tephras in Iceland. Holocene 9, 463-471.

Larsen, G., Eirfksson, J., Knudsen, K.L., Heinemeier, J., 2002. Correlation of late Holocene terrestrial and marine tephra markers, north Iceland: implications for reservoir age changes. Polar Res. 21, 283-290.

Lehman, R.M., Baker, K.E., Mattson, E.D., 2004. Distribution of microorganisms and their activities in capillary barriers implications for modelling of hydrologic transport through capillary barriers.. Vadose Zone J. 3, 134-142.

Li, X., Wai, O.W.H., Li, Y.S., Coles, B.J., Ramsey, M.H., Thornton, I., 2000. Heavy metal distribution in sediment profiles of Pearl River estuary. South China. Appl. Geochem. 15, 567-581.

Lowe, D.J., Hunt, J.B., 2001. A summary of terminology used in tephra- related studies. Les Dossiers de l'Archeo-Logis 1, 17-22.

Nachtegaal, M., Sparks, D.L., 2002. Kinetics and mechanisms of nickel surface precipitation in multi-sorbent systems: a spectroscopic study. In: Proceedings of the 17th World Congress of Soil Science, August 14-21, 2002, Bangkok, Thailand.

Oelkers, E., 2001. General kinetics description of multioxide silicate mineral and glass dissolution. Geochim. Cosmochim. Acta 65, 3703-3719.

Pollard, A.M., Blockley, S.P.E., Ward, K.R., 2003. Chemical alteration of tephra in the depositional environment: theoretical stability modelling. J. Quatern. Sci. 18, 79-93.

Price, N.B., Karageorgis, A.P., Kaberi, H., Zeri, C, Krasakopoulou, E., Voutsinou-Taliadouri, F., Lindsay, F., Assimakopoulou, G., Pagou, K., 2005. Temporal and spatial variations in the geochemistry of major and minor particulate and selected dissolved elements of Thermaikos Gulf, Northwestern Aegean Sea. Cont. Shelf Res. 25, 2428-2455.

Sadler, J.P., Grattan, J.P., 1999. Volcanoes as agents of past environmental change. Global Planet. Change 21, 181-196.

Schmincke, H.-U., Park, C, Harms, E., 1999. Evolution and environmental impacts of the eruption of Laacher See Volcano (Germany) 12,900 a PB. Quatern. Internat. 61, 61-72.

Shotyk, W., 1993. Ion chromatography of organic-rich natural waters from peatlands. I. Cl^- , NO_2^-, Br^-, NO_3^-, HPO_4^{2-} , SO_4^{2-} and oxalate. J. Chromatogr. 640, 309-316.

Soulier, A., 1995. Les formes solides du fer dans un sols hydromorphes, approche géochimique, micromorphologique et minéralogique. Ph.D. Thesis, Ecole Supérieure Agronomique de Rennes, Rennes, France.

Sparks, R.S.J., Bursik, M.I., Carey, S.C., Glaze, L., Gilbert, J.S., Woods, A.W., 1997. Volcanic plumes. John Wiley and Sons Inc., Hoboken, NJ, USA.

Steinmann, P., Shotyk, W., 1995. Ion chromatography of organic-rich natural waters from peatlands III. Improvements for measuring anions and cations. J. Chromatogr. A 706, 281-286.

Sterckeman, T., Douay, F., Baize, D., Fourrier, H., Proix, N., Schwartz, C, 2006. Trace elements in soils developed in sedimentary materials from Northern France. Geoderma, 136: 912-929.

Stipp, S.L.S., Hansen, M., Kristensen, R., Hochella Jr., M.F., Bennedsen, L., Dideriksen, K., Balic-Zunic, T., Leonard, D., Mathieu, H.-J., 2002. Behaviour of Fe-oxides relevant to contaminant uptake in the environment. Chem. Geol. 190, 321-337.

Techer, I., Advocat, T., Lancelot, J., Liotard, J.-M., 2001. Dissolution kinetics of basaltic glasses: control by solution chemistry and protective effect of the alteration film. Chem. Geol. 176, 235-263.

Thorarinsson, S., 1958. The Öraefajökull eruption of 1362. Acta Nat. Isl. 2, 1-99. Thorarinsson, S., 1967. The eruption of Hekla 1947-1948: I. The eruptions of Hekla in historical times. A Tephrochronological Study. Visindafelag Islendinga, Reykjavik, pp. 1-183.

Thorseth, I.H., Furnes, H., Tumyr, O., 1995. Textural and chemical effects of bacterial activity on basic glass: an experimental approach. Chem. Geol. 119, 139-160.

Todorova, S.G., Siegel, D.I., Costello, A.M., 2005. Microbial Fe(III) reduction in a minerotrophic wetland - geochemical controls and involvement in organic matter decomposition. Appl. Geochem. 20, 1120-1130.

Warren, P.H., Ulff-Møllera, F., Hubera, H., Kallemeyna, G.W., 2006. Siderophile geochemistry of ureilites: a record of early stages of planetesimal core formation. Geochim. Cosmochim. Acta 70, 2104-2126.

Wastegärd, S., 2002. Early to middle Holocene silicic tephra horizons from Katla volcanic system, Iceland: new results from the Faroe Islands. J. Quatern. Sci. 17, 723-730.

Weiss, D., Shotyk, W., Rieley, Jack, Page, S., Gloor, M., Reese, S., Martinez-Cortizas, A., 2002. The geochemistry of major and selected trace elements in a forested peat bog, Kalimantan, SE Asia, and its implications for past atmospheric dust deposition. Geochim. Cosmochim. Acta 66, 2307-2323.

Wolff-Boenisch, D., Gislason, S.R., Oelkers, E., Putnis, C.V., 2004a. The dissolution rates of natural glasses as a function of their composition at pH 4 and 106, and temperatures from 25 to 74 °C. Geochim. Cosmochim. Acta 68, 4843-4858.

Wolff-Boenisch, D., Gislason, S.R., Oelkers, E., Putnis, C.V., 2004b. The effect of fluoride on the dissolution rates of natural glasses at pH 4 and 25 °C. Geochim. Cosmochim. Acta 68, 4571-4582.

Woo, M.K., Young, K., 2006. High arctic wetlands: their occurrence, hydrological characteristics and sustainability. J. Hydrol. 320, 432-450.

Xu, Y., Axe, L, Boonfueng, T., Tyson, T.A., Trivedi, P., Pandya, K., 2007. Ni(ll) complexation to amorphous hydrous ferric oxide: an X-ray absorption spectroscopy study. J. Colloid Interface Sci. 314, 10-17.